

Effect of Interacting Rarefaction Waves on Relativistically Hot Jets

Jin Matsumoto^{1,2,3}, Youhei Masada⁴, and Kazunari Shibata¹

ABSTRACT

The effect of rarefaction acceleration on the propagation dynamics and structure of relativistically hot jets is studied through relativistic hydrodynamic simulations. We emphasize the nonlinear interaction of rarefaction waves excited at the interface between a cylindrical jet and the surrounding medium. From simplified one-dimensional models with radial jet structure, we find that a decrease in the relativistic pressure due to the interacting rarefaction waves in the central zone of the jet transiently yields a more powerful boost of the bulk jet than that expected from single rarefaction acceleration. This leads to a cyclic in-situ energy conversion between thermal and bulk kinetic energies which induces radial oscillating motion of the jet. The oscillation timescale is characterized by the initial pressure ratio of the jet to the ambient medium, and follows a simple scaling relation $\tau_{\text{oscillation}} \propto (P_{\text{jet},0}/P_{\text{amb},0})^{1/2}$. It is confirmed from extended two-dimensional simulations that this radial oscillating motion in the one-dimensional system manifests as modulation of the structure of the jet in a more realistic situation where a relativistically hot jet propagates through an ambient medium. It is found that when the ambient medium has a power law pressure distribution, the size of the re-confinement region along the propagation direction of the jet in the modulation structure λ evolves according to a self-similar relation $\lambda \propto t^{\alpha/2}$ where α is the power-law index of the pressure distribution.

Subject headings: galaxies: jets — hydrodynamics — methods: numerical — relativistic processes — shock waves

1. Introduction

Relativistic jets are collimated bipolar outflows that have a velocity almost equal to light speed. They are ubiquitous among astrophysical systems consisting of a compact object sur-

¹Kwasan and Hida Observatories, Kyoto University, Kyoto, Japan; jin@kusastro.kyoto-u.ac.jp

²Department of Astronomy, Kyoto University, Kyoto, Japan

³National Astronomical Observatory of Japan, Tokyo, Japan

⁴Graduate School of System Informatics, Department of Computational Science, Kobe University, Kobe, Japan

rounded by an accretion disk, e.g., active galactic nuclei (AGNs; Ferrari 1998), microquasars (Mirabel & Rodríguez 1999) and the central engine of gamma-ray bursts (GRBs; Piran 2004; Mészáros 2006). Although there are many works that try to determine the mechanism by which relativistic jets are accelerated and collimated, the process is still not understood.

Aloy & Rezzolla (2006) recently reported that relativistic jets can be powerfully boosted along the interface between the jet and ambient medium, if the jet has sufficiently large velocity and specific enthalpy, and is overpressured (see also Aloy et al. 2003, 2005). A rarefaction wave excited at the interface converts the relativistic thermal energy of the plasma into kinetic energy and yields an amplification of the Lorentz factor in the jet-ambient medium interface. This type of boost, which we label rarefaction acceleration, is not possible in Newtonian dynamics, but is an inherent process in relativistic hydrodynamics.

The relativistic magnetohydrodynamic effects on the rarefaction acceleration were studied by Mizuno et al. (2008) and Aloy & Mimica (2008). Mizuno et al. (2008) showed that, especially in the case of a magnetic field perpendicular to the jet direction, the boost becomes more powerful than that expected from pure hydrodynamic models. Aloy & Mimica (2008) studied the radiative output of magnetized jets bounded by anomalous shear layers in which jets are boosted due to the rarefaction wave. It was indicated theoretically that the boosted Lorentz factor is well described, as a function of the initial pressure ratio between the jet and the ambient medium, by a simple scaling law derived by Zenitani et al. (2010) (see also Komissarov et al. 2010).

Rarefaction acceleration of jets is a process that is expected to occur under realistic conditions. Since a large amount of energy is stored in the jet at its launch site, the jet would be initially overpressured. Actually, the jet from AGNs often appear to be overpressured with relativistic velocity even as it propagates through the interstellar medium (Bicknell & Begelman 1996). In some cases it has two components: a faster, lighter component surrounded by a slower, denser component (Giroletti et al. 2004; Meliani & Keppens 2009). The jet that emerges from the central engine of GRBs is also expected to be hot and overpressured when it propagates inside the progenitor star. Furthermore, the fluid of the boundary layer of the jet would be boosted by rarefaction acceleration when the relativistic jet breaks out on the surface of the progenitor star and the external pressure support drops (Tchekhovskoy et al. 2010). The Lorentz factor of the jet can be boosted when it enters the low pressure region outside of the thick accretion torus which is a possible candidate of the central engine of short GRBs (Aloy et al. 2005).

In this paper, we study in detail how the rarefaction acceleration affects the propagation dynamics of relativistically hot jets through one-dimensional (1D) and two-dimensional (2D) relativistic hydrodynamic simulations. The nonlinear interaction of rarefaction waves excited at the interface between the jet and ambient medium is especially focused upon because it might have a potential impact on the boosting process and even alter the dynamics and structure of the jet. This

paper is organized as follows. In Section 2, the numerical results of our 1D relativistic hydrodynamic simulations are presented. We perform 2D simulations in Section 3. Finally, we discuss and summarize our findings in Section 4 and 5.

2. One-dimensional Simulations

2.1. Numerical Models and Setup

In order to investigate the interaction of rarefaction waves excited at the jet-ambient medium interface, we initially set a jet surround by ambient gas in the calculation domain, as is schematically shown in Figure 1. We solve the special relativistic hydrodynamic (RHD) equations in a one-dimensional axisymmetric cylindrical coordinate system. The fluid velocity has two components: the normal velocity v_r and tangential velocity v_z to the interface which separates the jet and ambient medium. Derivatives of the physical variables in the z -direction are assumed to be zero. We adopt, as the equation of state for the relativistic gas, the ideal gas law with a ratio of specific heats $\Gamma = 4/3$. The basic equations are then,

$$\frac{\partial}{\partial t}(\gamma\rho) + \frac{1}{r} \frac{\partial}{\partial r}(r\gamma\rho v_r) = 0, \quad (1)$$

$$\frac{\partial}{\partial t}(\gamma^2 \rho h v_r) + \frac{1}{r} \frac{\partial}{\partial r} \left[r(\gamma^2 \rho h v_r^2 + P c^2) \right] = \frac{P c^2}{r}, \quad (2)$$

$$\frac{\partial}{\partial t}(\gamma^2 \rho h v_z) + \frac{1}{r} \frac{\partial}{\partial r} \left[r(\gamma^2 \rho h v_z v_r) \right] = 0, \quad (3)$$

$$\frac{\partial}{\partial t}(\gamma^2 \rho h - P) + \frac{1}{r} \frac{\partial}{\partial r} \left[r(\gamma^2 \rho h v_r) \right] = 0. \quad (4)$$

where $\gamma \equiv 1/\sqrt{1-(v_x/c)^2-(v_z/c)^2}$ is the Lorentz factor and $h = c^2 + \Gamma P/(\Gamma - 1)\rho$ is the specific enthalpy. The other symbols have their usual meanings.

For our initial conditions, we assume a relativistically hot jet with larger pressure and smaller rest-mass density than the ambient medium. The initial density and pressure in the jet are chosen as $\rho_{\text{jet},0} = 0.1$ and $P_{\text{jet},0} = 1$, respectively. Those of the ambient medium are $\rho_{\text{amb},0} = 1$ and $P_{\text{amb},0} = 0.1$. In addition, the jet velocity to the z -direction is relativistic $v_{\text{jet},0} = 0.99c$, with a Lorentz factor of $\gamma_{\text{jet},0} \sim 7$. The ambient medium does not move and the normal velocity v_r is set to be zero initially in the calculation domain. In this paper, we set a simple model for the jet-ambient medium system in order to investigate the basic physics of the interaction of rarefaction waves excited at the jet-ambient medium interface.

The normalization units in length, velocity, time, and energy density are chosen as the initial jet width $W_{\text{jet},0}$, light speed c , light crossing time over the initial jet width $W_{\text{jet},0}/c$, and rest mass

energy density in the ambient medium $\rho_{\text{amb},0}c^2$. The computational domain spans $0 < r < 2$. A uniform grid with a grid size $\Delta r = 10^{-3}$ is adopted for our calculations. We use a reflecting boundary condition on the axis $r = 0$. The outer boundary of the grid uses the outflow (zero gradient) boundary condition.

We use a relativistic HLLC scheme for hydrodynamics to solve the RHD equations (Mignone & Bodo 2005). The primitive variables are calculated from the conservative variables following the method of Mignone & McKinney (2007). We use a MUSCL-type interpolation method to attain second-order accuracy in space while the temporal accuracy obtains second-order by using Runge-Kutta time integration.

2.2. Results of One-dimensional Simulations

2.2.1. *The Jet Boosting Mechanism of Aloy & Rezzolla 2006*

Since the jet is initially hotter and has a higher pressure than the denser, colder ambient medium, three types of hydrodynamic wave are excited at the jet-ambient medium interface. A shock wave propagates outward through the ambient medium, and a rarefaction wave starts to travel toward the center of the jet. Behind the shock wave, there exists a contact discontinuity, that is an entropy wave, corresponding to the edge of the jet. The pressure decrease in the jet due to the rarefaction wave accelerates the gas in the jet-ambient medium interface in the tangential direction as a natural outcome of relativistic hydrodynamics, as was reported by Aloy & Rezzolla (2006).

Following the analysis of Zenitani et al. (2010), by combining Equations (3) and (4) we can obtain

$$\begin{aligned} \gamma^2 \rho h \left(\frac{\partial}{\partial t} + v_r \frac{\partial}{\partial r} \right) \frac{v_z}{c} &= - \frac{v_z}{c} \frac{\partial P}{\partial t} \\ &\sim - \frac{\partial P}{\partial t} \quad (\because v_z \sim c). \end{aligned} \quad (5)$$

This indicates that a time-decreasing pressure is responsible for the acceleration of the gas in relativistic hydrodynamics, unlike the non-relativistic case. The conversion from the thermal energy to bulk kinetic energy of the jet is then constrained by the relativistic Bernoulli equation which provides enthalpy conservation,

$$\gamma h \sim \text{const.} \quad (6)$$

The relativistic jet is accelerated by this mechanism, found by Aloy & Rezzolla (2006), in our numerical model.

2.2.2. Temporal Evolution of the System

Figure 2 shows the temporal evolution of our jet-ambient medium system. The color contour represents the spatial distribution of (a) the density ρ , (b) the pressure P , (c) the radial velocity v_r , (d) the tangential velocity v_z , and (e) the Lorentz factor γ . Snapshots of the spatial distribution of the hydrodynamics variables at the time $t=5, 27, 43$ and 57 are illustrated in Figure 3, 4, 5 and 6, respectively. The dashed line in these figures denote the profiles of hydrodynamic variables at the time $t = 0, 17, 33,$ and 50 for the better demonstration of the propagation of the rarefaction and shock waves. In the early evolutionary stage ($0 < t < 5$: phase (i)), described in section 3.3.1, the single rarefaction acceleration of the gas is observed in the jet-ambient medium interface. Figure 3 gives the spatial distribution of the jet-ambient medium system at $t = 0, 1$ and 5 . The Lorentz factor of the fluid at the jet-ambient interface is boosted to 12 due to the rarefaction acceleration when $t=1$ and 5 . One can find that the contact discontinuity moves outward, that is, the jet expands since the contact discontinuity corresponds to the edge of the jet. Note that the head of the rarefaction wave intersects the jet axis while the Lorentz factor of the fluid inside the jet reaches its maximum value at the tail of the rarefaction wave when $t = 5$.

Subsequently at $t \simeq 5$ the rarefaction waves converge on the central region of the jet and an incident shock wave is excited at the tail of the rarefaction wave in the cylindrical jet, bringing a substantial change in the dynamics (phase (ii) in Figure 2). The shock wave is excited at the tail of the rarefaction wave as a natural result of the cylindrical shock tube problem in which the characteristic lines intersect. The shock wave is located at $r = 1$ when $t = 17$ as shown in Figure 4. The gas pressure in the interacting region of rarefaction waves, confined by the surface of the shock wave, is then further reduced and becomes lower than that of the ambient gas (see Figure 4). Since, according to Equation (5), the thermal energy is converted to the bulk kinetic energy of the gas, the Lorentz factor of the gas in the interacting region is further boosted. The peak Lorentz factor of the gas inside the rarefaction region reaches $\gamma \simeq 60$ at $t = 44$ (see Figure 5), which is a factor $\simeq 5$ higher than that due to the single rarefaction acceleration at the jet-ambient medium interface. The boosted Lorentz factor of the fluid at the jet-ambient medium interface due to the single rarefaction acceleration is roughly 12 as shown in Figure 3, 4, 5, and 6.

The interaction of rarefaction waves generates a strong inward pressure gradient behind the jet-ambient medium interface which acts to decelerate the radial expansion of the jet, turning expansion of the jet into contraction around time $t = 27$ (see Figure 2(a), 2(c)). The contraction of the contact discontinuity results in converging flows inside the jet in the phase (iii).

When $t = 44$, the inward shock waves proceeding the converging flow collide with each other at the center of the jet and propagate outward. The gas bounded by the shock is compressed and heated. Since according to Equation (5) a time-increasing pressure decelerates the tangential velocity of the jet, the Lorentz factor of the jet reduces and the specific enthalpy increases (see

Equation (6)). Thus, in phase (iv), the Lorentz factor of the shock heated gas drops. The spatial distribution of the jet-ambient medium system at the end of the phase (iv) ($t = 57$) is demonstrated in Figure 6.

When the shock wave encounters the contact discontinuity around $t = 58$, the system has almost returned to its initial state. The jet still has a sufficiently larger tangential velocity and specific enthalpy than the ambient medium, but the gas pressure in the jet, however, has become smaller than that of the initial state. This is the result of the energy conversion from thermal energy to bulk kinetic energy of the jet. Since the system is restored to a state that is almost the same as the initial conditions, the three types of hydrodynamic waves, an outward propagating shock wave, a contact discontinuity (the edge of the jet), and a converging rarefaction wave, appear at the jet-ambient medium interface. Therefore the contracting radial motion of the jet becomes an expanding motion.

2.2.3. *Oscillation of the Relativistic Jet*

After phase (iv), the system has returned to conditions similar to the initial conditions, and the system repeats the cycle of phases (i)–(iv) until the pressure of the jet becomes equal to that of the ambient gas. During the cycle, the radial motion of the jet oscillates between expansion and contraction, and the system undergoes successive exchanges between thermal energy and kinetic energy. Figure 7 shows the temporal evolution of (a) the jet width, (b) the maximum and average tangential velocity, (c) the maximum and average Lorentz factor, and (d) the average of the specific enthalpy in the jet. The oscillations of the Lorentz factor and the averaged specific enthalpy are in anti-phase in accordance with the relativistic Bernoulli relation (6).

When the pressure inside the jet becomes almost equal to the ambient gas around time $t = 1000$, the oscillation of the jet ends. The spatial distributions of the density, pressure, radial and tangential velocity and Lorentz factor at $t = 2000$ are depicted in Figure 8. At the quasi-steady state, there exists an accelerated region localized to the boundary layer of the jet, as is shown in Figure 8(d) and (e). The physical parameters in the interface of the jet are comparable to those expected from single rarefaction acceleration (Aloy & Rezzolla 2006). This is because the oscillating motion during the relaxation stage, shown in Figure 7, has little influence on the physical parameters in the boundary layer. At the final quasi-steady state, the pressure in the jet is the almost same as that of the ambient medium. The initial relativistic thermal energy of the jet is converted into the bulk kinetic energy of the jet.

2.3. Scaling Law for the Oscillation Timescale

As shown in the section 2.2.3, the initial non-equilibrium system evolves, through a transition stage, toward a quasi-steady state where a hydrostatic balance is established in the radial direction. During the transition stage, the oscillation timescale is almost constant while the oscillation amplitude gradually decreases. In this section, we derive a scaling relation which can reproduce the oscillation timescale of our jet-ambient medium system.

Figure 7(a) indicates that, during the transition stage, the radial size of the jet oscillates around the jet width of the final quasi-steady state. We then approximate the typical oscillating width of the jet by the jet width of the saturated state illustrated in Figure 8. The typical oscillation time of the jet would be determined by the propagation time of the sound waves over the typical oscillating width of the jet. When using the physical parameters at the quasi-steady state, the oscillating time is evaluated as

$$\tau = \bar{\gamma}_{\text{jet},s} W_{\text{jet},s} / C_s \quad (7)$$

in the laboratory frame. Here, the subscript s stands for the physical values in the final steady state. Since the thermal energy inside the jet is relativistic, the sound speed is well approximated by $C_s \simeq c/\sqrt{3}$.

In order to derive the typical oscillation time of the jet-ambient medium system, we need to estimate the average Lorentz factor in the jet $\bar{\gamma}_{\text{jet},s}$ in the quasi-steady state. Since the total energy in the jet is almost conserved during the transition phase¹, we can obtain the following relation neglecting the rest mass energy, which is smaller than the relativistic thermal energy in the jet,

$$W_{\text{jet},s}^2 \bar{\gamma}_{\text{jet},s}^2 P_{\text{amb},0} = W_{\text{jet},0}^2 \gamma_{\text{jet},0}^2 P_{\text{jet},0} . \quad (8)$$

Note that we replace the pressure in the jet in the steady state $P_{\text{jet},s}$ with that of the initial ambient medium $P_{\text{amb},0}$ because a pressure balance is established between inside and outside the jet in the final quasi-steady state.

From Equations (7) and (8), we can give the scaling law for the oscillation time

$$\tau = \sqrt{3} \gamma_{\text{jet},0} \left(\frac{W_{\text{jet},0}}{c} \right) \left(\frac{P_{\text{jet},0}}{P_{\text{amb},0}} \right)^{1/2} . \quad (9)$$

In Figure 9, we plot the oscillation time averaged over ten cycles for numerical runs with different initial pressure ratios. The solid line represents the analytic scaling we derived. This indicates that our numerical results are well captured by our simple scaling law shown in Equation (9).

¹Our models indicate that the loss of the total energy is less than 0.4% in the transition phase

Magnetic fields, which are expected to exist in relativistic jets from AGNs and GRBs (Blandford & Payne 1982; Uchida & Shibata 1985; Shibata & Uchida 1986; Blandford 2000; Lyutikov & Blandford 2003), may alter the oscillation mechanism we have presented. In the poynting flux jet, the magnetic pressure is dominant over the gas pressure. Since the sum of the magnetic pressure and the gas pressure contributes to the rarefaction acceleration (Mizuno et al. 2008; Aloy & Mimica 2008; Zenitani et al. 2010; Tchekhovskoy et al. 2010; Komissarov et al. 2010), it is expected that the magnetic pressure would play much the same role as the relativistic thermal pressure in the jet oscillation.

3. Two-dimensional Simulations

3.1. Numerical Models and Setup

We investigate how the oscillating motion found in the 1D model affects the propagation dynamics and the structure of the jet in a more realistic two dimensional axisymmetric system. Our axisymmetric simulation of the jet propagation has been carried out in cylindrical coordinates (r, z) , where the z -axis coincides with the symmetric axis (see Figure 1). Relativistically hot flow is continuously injected into the ambient medium from the lower boundary of the computational domain, $z = z_{\text{low}}$. The governing equations we solved are

$$\frac{\partial}{\partial t}(\gamma\rho) + \frac{1}{r}\frac{\partial}{\partial r}(r\gamma\rho v_r) + \frac{\partial}{\partial z}(\gamma\rho v_z) = 0, \quad (10)$$

$$\frac{\partial}{\partial t}(\gamma^2\rho h v_r) + \frac{1}{r}\frac{\partial}{\partial r}\left[r(\gamma^2\rho h v_r^2 + Pc^2)\right] + \frac{\partial}{\partial z}\left[\gamma^2\rho h v_r v_z\right] = \frac{Pc^2}{r}, \quad (11)$$

$$\frac{\partial}{\partial t}(\gamma^2\rho h v_z) + \frac{1}{r}\frac{\partial}{\partial r}\left[r(\gamma^2\rho h v_z v_r)\right] + \frac{\partial}{\partial z}\left[\gamma^2\rho h v_z^2 + Pc^2\right] = 0, \quad (12)$$

$$\frac{\partial}{\partial t}(\gamma^2\rho h - P) + \frac{1}{r}\frac{\partial}{\partial r}\left[r(\gamma^2\rho h v_r)\right] + \frac{\partial}{\partial z}\left[\gamma^2\rho h v_z\right] = 0, \quad (13)$$

where we use the same normalization units and symbols defined in section 2 in order to compare the results of 1D and 2D calculations. The injection flow has the same hydrodynamic parameters as the 1D model, that is $\rho_{\text{jet},0} = 0.1$, $P_{\text{jet},0} = 1.0$, $v_{r,0} = 0$, $v_{z,0} = 0.99c$, and $\gamma_{\text{jet},0} \sim 7$.

For the simulation presented here, we use simple power law models for the ambient medium. When assuming a polytropic atmosphere, the ambient medium has pressure and density distribu-

tions

$$P_{\text{amb}} = P_{\text{amb},0} \left(\frac{\hat{r}}{W_{\text{jet},0}} \right)^{-\alpha} \quad (14)$$

$$\rho_{\text{amb}} = \rho_{\text{amb},0} \left(\frac{\hat{r}}{W_{\text{jet},0}} \right)^{-3\alpha/4}, \quad (15)$$

where $\hat{r} = \sqrt{r^2 + z^2}$ is the spherical radius in the cylindrical coordinate system and $P_{\text{amb},0} = 0.1$ and $\rho_{\text{amb},0} = 1$. Note that the model with $\alpha = 0$ corresponds to a uniform ambient medium model. For simplicity we neglect the effect of the gravity and the ambient medium does not move initially in the calculation domain. We set the power law index of the ambient medium α as 0.0, 0.4, and 0.8 in the following simulations.

The calculation domain spans $(100W_{\text{jet},0} \times 1500W_{\text{jet},0})$ in the $(r \times z)$ -plane which corresponds to a 1600×24000 grid. A uniform resolution of 8 numerical cells over the radius of the injection jet is used. At the lower boundary ($z_{\text{low}} = 1$) hydrodynamic variables are fixed inside the jet injection region ($0 < r < 0.5$) while the boundary conditions are reflective outside the jet injection region. An outflow boundary condition is imposed on the outer boundaries of the grid and the symmetry axis is reflecting.

3.2. Analytic Estimation: The Size of Cusp-Shaped Boosted Region

Our one-dimensional models suggest that the relativistically hot jet alternates between acceleration and deceleration phases with the oscillation period derived in Equation (9) when it propagates through a uniform ambient medium. This is a consequence of the in-situ conversion between thermal and bulk kinetic energies inside the jet. When the relativistically hot jet is continuously injected into the ambient medium in more realistic multi-dimensional situations, we can expect that the radial oscillating motion that appeared in the one-dimensional system manifests as the periodically modulated structure of the jet along the jet propagation direction. From the scaling law for the oscillation period of the jet obtained in section 2.3, we estimate here the typical size of the region where the relativistic jet is boosted.

The space-time diagram of Figure 2 shows the boosted region of the jet has a cusp shape which corresponds to the interacting region of rarefaction waves. The multi-dimensional extension of this jet oscillation in the 1D system would provide the periodic formation of the cusp-shaped boosted region confined by oblique shocks (Norman et al. 1982; Sanders 1983) along the propagation direction of the jet. In previous numerical works, shock waves confining the flow to a narrow region are observed inside relativistic jets, that is called the reconfinement shock (e.g., Marti et al. 1997; Gomez et al. 1997; Komissarov & Falle 1997, 1998; Aloy et al. 2000a,b; Agudo et al. 2001;

Zhang et al. 2003, 2004; Mizuta et al. 2006; Mizuta & Aloy 2009; Perucho & Martí 2007; Morsony et al. 2007, 2010; Lazzati et al. 2009; Mimica et al. 2009; Nagakura et al. 2011). The cusp-shaped boosted region, which is result from the jet oscillation due to the interacting rarefaction waves, would appear in the multi-dimensional system as the reconfinemet region found in these previous works.

We can approximate the size of the cusp-shaped boosted region, that is the reconfinemet region, by the propagation distance of the jet fluid during the typical oscillation time τ written in equation (9). Since the fluid velocity of the relativistic jet is almost equal to the speed of light, the propagation distance λ is given by

$$\lambda = c\tau = \sqrt{3}\gamma_{\text{jet},0}W_{\text{jet},0}\left(\frac{P_{\text{jet},0}}{P_{\text{amb},0}}\right)^{1/2}. \quad (16)$$

The size of the reconfinemet region is proportional to the Lorentz factor of the injected jet and the square root of the initial pressure ratio between the jet and ambient medium. When the relativistically hot jet is injected continuously into the uniform ambient medium, the cusp-shaped reconfinemet region with the size λ will be formed periodically inside the jet. The scaling law which relates the typical size of the reconfinemet region to the pressure of the ambient medium is also analytically derived by Daly & Marscher (1988). We compare our scaling to it later in the discussion section.

In a gravitationally bounded atmosphere, which is plausible in the central engine of relativistic jets, the ambient gas should be stratified and have a pressure distribution along the propagation direction of the jet. Since the radial oscillation of the relativistic jet is controlled by the pressure ratio between the jet and ambient medium, the size of the reconfinemet region λ evolves with time when the jet propagates through the stratified medium. Adopting the pressure profile for the stratified ambient medium described by equation (14), the size of the reconfinemet region along the z -axis is evaluated as

$$\lambda = \sqrt{3}\gamma_{\text{jet},0}W_{\text{jet},0}\left(\frac{P_{\text{jet},0}}{P_{\text{amb},0}}\right)^{1/2}\left(\frac{z}{W_{\text{jet},0}}\right)^{\alpha/2}. \quad (17)$$

Since the fluid velocity inside the reconfinemet region should be relativistic, we can provide the following relation by replacing z in equation (17) with ct ,

$$\lambda \propto t^{\alpha/2}. \quad (18)$$

This implies that the cusp-shaped reconfinemet region evolves self-similarly in the multi-dimensional system (see also Komissarov & Falle 1998; Bromberg & Levinson 2007; Nalewajko & Sikora 2009; Kohler et al. 2011).

3.3. Self-Similar Evolution of Reconfinement Region

3.3.1. Uniform Ambient Medium Model

Figure 10 shows the temporal evolution of the injected relativistically hot jet for a uniform ambient model (power-law index $\alpha = 0$ in equations (14) and (15)) in the early evolutionary stage. The color contour represents the spatial distribution of (a) the density ρ , (b) the pressure P , and (c) the Lorentz factor γ when $t = 100$ (left), 200 (middle), and 300 (right) respectively. As expected from one-dimensional models, the cusp-shaped rarefaction regions confined by oblique shocks are formed inside the jet. In those regions, the fluid of the jet is accelerated due to the interaction of rarefaction waves and subsequent in-situ energy conversion from relativistic thermal energy to bulk kinetic energy (see Section 2.2). Since the rarefaction waves are repeatedly excited behind the jet head, the reconfinement regions are periodically formed along the jet-propagation direction and create the modulated structure of the jet in the early evolutionary stage.

Figure 11 gives the spatial distribution of (a) the density ρ , (b) the pressure P and (c) the Lorentz factor γ when $t = 2000$. As the jet propagates, the modulated structure of the jet has a loss in coherency except at the region near the injection point. This is because there are vortices that are episodically created by a Kelvin-Helmholtz like instability that develops between the jet and the backflow near the jet head (Mizuta & Aloy 2009). Since the continuously induced vortices make the ambient medium inhomogeneous, the modulation structure of the jet becomes incoherent and then the size of the reconfinement region violently fluctuates, except the region near the injection point where the ambient inhomogeneity remains relatively weak.

The spatial distribution of the Lorentz factor near the jet injection point is shown in Figure 12(b). In order to compare it to the result of the 1D calculation, the temporal evolution of the Lorentz factor in the jet-ambient system of 1D simulation is shown in Figure 12(a). The size of the cusp-shaped rarefaction region in both cases seems to be almost the same, although the vertical axis is the time in Figure 12(a). The typical size of the reconfinement region in the jet-propagation direction can be estimated theoretically from relation (16). With using the parameters $\gamma_{\text{jet},0} \simeq 7$, $W_{\text{jet},0} = 1$, and $P_{\text{jet},0}/P_{\text{amb},0} = 10$, we can obtain $\lambda \simeq 40$, indicating our scaling relation captures the result of 2D simulation. The width of the contact layer of 2D simulation is larger than that of the 1D calculation due to the lower resolution of the simulation.

The pressure on the z -axis in the 1D and 2D simulations is shown in Figure 13(a) and (b), respectively. Note that the horizontal axis represents the time t in Figure 13(a) and (b) depicts the pressure in a 1D cut along the z -axis of Figure 11(b). In 1D models, the oscillation of the jet is a transient phenomena and terminated when the pressure inside the jet falls to the same level as that of the ambient medium (See section 2.2.3). On the other hand, in 2D case, the pressure inside the jet continues to vary and a pressure balance between the jet and the ambient medium is not

achieved. The predicted size of the reconfinement region apparently seems to exist only near the injection point.

Figure 14 shows the time-distance diagram for the pressure along the z -axis. The reconfinement region near the injection point does not move with time while the reconfinement region formed behind the jet head propagates along the jet direction. Though the modulation properties of the jet change due to the ambient medium inhomogeneity, the typical size of the reconfinement region is expected to be maintained at a constant value at any time as shown in Figure 14.

The temporal evolution of the Fourier spectrum of the pressure measured along the jet axis is given in Figure 15. Here the Fourier transformation $P(k)$ is obtained from

$$P(k) = \frac{1}{L_{\text{jet}}} \int_0^{L_{\text{jet}}} P_{z\text{-axis}}(z) \exp^{-ikz} dz, \quad (19)$$

where L_{jet} is the length of the jet in the propagation direction. The solid, dashed and dotted curves indicate the spectra at the different phases $t = 600, 1200$ and 2000 , respectively. Despite the different evolutionary phase, all the spectra show a peak at around $k/2\pi \simeq 1/40$ which corresponds to the inverse of the typical size of the reconfinement region derived from equation (16) and we can find that there is a second harmonic in each spectrum. This suggests that the typical size of the reconfinement region inside the jet is essentially determined by the modulation caused by the interaction of rarefaction waves even though the ambient medium inhomogeneity causes fluctuation in jet structure.

3.3.2. Power-law Models

There is one main important difference between the power law models with $\alpha \neq 0$ and the uniform ambient model ($\alpha = 0$). For the models with decreasing pressure profile with distance from the launching point of the jet, the jet expands more than in the uniform ambient model. The jet is then further accelerated because the pressure inside the reconfinement region decreases more drastically and a larger amount of thermal energy is converted into bulk kinetic energy.

Figure 16 shows the temporal evolution of the injected relativistically hot jet for the power law ambient medium model with $\alpha = 0.8$. The meanings of the color contours and the columns are the same as those of Figure 10. Note that the vertical and horizontal scale of Figure 16 is 2.5 times larger than that of Figure 10. It is found that, though the inflow flux is the same for each model, the maximum Lorentz factor inside the reconfinement region reaches $\simeq 180$ for the power-law model with case $\alpha = 0.8$, while it is $\simeq 45$ for the uniform ambient medium model (see Figure 10(c) and Figure 12(b)).

The decreasing ambient pressure results in a longer oscillation timescale as suggested in equation (9). The size of the reconfinement region in the power law models thus becomes larger than that in the uniform ambient medium model. Additionally, the results shown in Figure 16 imply that the reconfinement region evolves self-similarly.

In order to confirm the self-similarity, we investigate the time trajectory of the cusp of the reconfinement region on the jet axis, depicted by diamonds in Figure 17, after the cusp-shaped region is formed. Overplotted on Figure 17 is the curve denoting the scaling relation (18) which is obtained from the results of the 1D models (see section 3.2). Panels (a) and (b) correspond to the cases with $\alpha = 0.4$ and 0.8 respectively. These figures confirm that the reconfinement region evolves self-similarly once the cusp-shaped reconfinement region is formed.

4. Discussion

Aloy & Rezzolla (2006) discussed, for the first time, a new mechanism in relativistic hydrodynamics that can act as a powerful booster in jets, that is rarefaction acceleration. This mechanism is purely hydrodynamical and operates when the jet-ambient system satisfies three physical conditions, that is, the jet should be hot and overpressured, and have a relativistic velocity to the jet-ambient medium interface. The hot jet stores an internal energy comparable to or larger than its rest mass energy. When the pressure of the jet is larger than that of the ambient medium, the rarefaction wave is excited at the jet-ambient medium interface and the relativistic thermal energy of the plasma can be converted into the bulk kinetic energy of the jet near the interface. An expansion of the relativistically hot jet to the underpressured ambient medium is responsible for the rarefaction acceleration of the jet.

The rarefaction acceleration should be commonly operated in the jet which satisfies these conditions, and which have been observed in many previous simulations as expected (e.g., Gomez et al. 1997; Aloy et al. 2000b; Scheck et al. 2002; Zhang et al. 2003). The reconfinement region confined by the oblique shock has been also formed in these previous simulations as a natural outcome of the rarefaction acceleration in the multidimensional system. However, the rarefaction acceleration can not be observed in the cold jet where the internal energy of the fluid is less than the rest mass energy of the fluid even if it shows the reconfinement shock (e.g., Komissarov & Falle 1997).

Daly & Marscher (1988) explored the dynamics of relativistic, hot and overpressured jets on the basis of a simplified, quasilinear, hydrodynamic equations for adiabatic, steady, cylindrically symmetric, and irrotational flows. In that work, they have already found the variety of flow structures with oscillating cross section or standing shocks. In addition, they have discussed scaling laws which relate the intrinsic properties of the jet to the pressure of the ambient medium.

In this sense, our finding is that there exists a close connection between the rarefaction acceleration mechanism discussed by Aloy & Rezzola and the flow structure with the reconfinement region and oscillating cross section quantitatively by using 1D and 2D hydrodynamic simulations. It is remarkable that simple 1D model based on Aloy & Rezzola (2006)’s mechanism can reproduce complicated 2D structure of jets not only in rarefaction acceleration region but also in the reconfinement region so well. Since 1D model is simple and easy to understand, these findings would be useful for more detailed study of jets.

It should be finally emphasized that the scaling law we obtained in this work (equation (16)) is different from that found by Daly & Marscher (1988). This would be because the approximations used for deriving the scaling in their work is applicable only to the system with a small pressure difference between the jet and ambient medium. Our scaling law can capture the flow properties of the jet-ambient medium system in the wider parameter range than that covered by the scaling law of Daly & Marscher (1988).

The simple scaling law for the self-similarity of the reconfinement region (18) would predict the evolution of the reconfinement region in the context of both AGN jets and GRBs. The reconfinement shocks due to the interacting rarefaction waves may be able to account for the confinement of the relativistic jet from AGN on a sub-parsec scale (Junor et al. 1999; Kovalev et al. 2007; Acciari et al. 2009). Some authors propose that the radio knots in the jet may correspond to reconfinement regions (e.g., Daly & Marscher 1988; Gomez et al. 1995; Bicknell & Begelman 1996; Komissarov & Falle 1997; Stawarz et al. 2006; Mimica et al. 2009). The scaling law (18) predicts that radio knots in the jet from AGNs evolve self-similarly with time depending on the power law index of the ambient pressure distribution when the relativistically hot and steady jet is formed near the central engine.

Although the numerical work in this paper are based on simulations with a constant engine which powers the jet, the variability injected by the central engine also leads to inhomogeneity in relativistic jets (Gomez et al. 1997; Mimica et al. 2009; Morsony et al. 2010). This might be a promising mechanism for generating internal shocks in relativistic jets, accounting for the time-variable emission properties of AGNs and GRBs (Takahashi et al. 2000; Piran 2004; Mimica et al. 2005; Mészáros 2006). The relation for inhomogeneity in the jet between the variability injected by the central engine and the interaction of the relativistic jet with the ambient medium is also needed to be investigated in a more realistic situation. Actually, for the case of power-law ambient models, we need a larger calculation domain while retaining the same resolution to study the effect of the vortices developed around the jet head on the propagation dynamics of the jet. This is because the jet expands more rapidly and the modulation structure becomes larger as the power-law index α increases. However, these studies go beyond the scope of this paper, but will be studied in a separate paper.

5. Summary

The nonlinear evolution of the interacting rarefaction waves excited at the cylindrical jet-ambient medium interface is studied through one-dimensional relativistic hydrodynamic simulations. It is found that an enhanced decrease in the relativistic pressure due to the interaction of rarefaction waves transiently yields a more powerful boost of the Lorentz factor of the bulk jet than that expected from a single rarefaction wave. The cyclic in-situ energy conversion between thermal energy and bulk kinetic energy is a natural relativistic outcome of the jet scenario studied and responsible for the radial oscillating motion of the jet. The oscillation timescale is characterized by the initial pressure ratio of the jet to the ambient medium, and follows a simple scaling relation $\tau_{\text{oscillation}} \propto (P_{\text{jet},0}/P_{\text{amb},0})^{1/2}$.

It is confirmed from extended two-dimensional simulations that repeated excitation and convergence of rarefaction waves result in the alignment of the interacting regions of rarefaction waves, confined by oblique shocks, along the propagation direction of the jet when a relativistically hot jet propagates through an ambient medium. The evolution of the reconfinement region in which the fluid of the jet is powerfully boosted due to the interacting rarefaction waves has a self-similar property when the relativistic jet propagates through the ambient medium which has a power law pressure distribution. The evolution of the size of the reconfinement region along the jet direction λ follows a simple scaling law $\lambda \propto t^{\alpha/2}$ where α is the power law index of the pressure distribution. Especially, in the uniform ambient medium model ($\alpha = 0$) the typical size of the reconfinement region inside the jet is essentially determined by the modulation caused by the interaction of rarefaction waves.

We thank Hiroyuki R. Takahashi and Akira Mizuta for thier useful discussions. We thank Andrew Hillier for his careful reading of the manuscript. This work was supported by the Grant-in-Aid for the global COE program “The Next Generation of Physics, Spun from Universality and Emergence” from the Ministry of Education, Culture, Sports, Science and Technology (MEXT) of Japan. Numerical computations were carried out on Cray XT4 at Center for Computational Astrophysics, CfCA, of National Astronomical Observatory of Japan and on SR16000 at YITP in Kyoto University. J.M. acknowledges support by the Research Fellowship of the Japan Society for the Promotion of Science (JSPS).

A. Convergence Tests

A.1. One-dimensional Riemann Problem with Transverse Velocity

The 1D relativistic Riemann problem with large transverse velocity requires high resolution in order to numerically resolve the complicated structure (Zhang & MacFadyen 2006; Mizuta et al. 2006; Mizuno et al. 2008). We have tested our code on a 1D (x -direction) Riemann problem with transverse velocity using uniform resolutions of $\Delta x = 10^{-3}$ and 2×10^{-5} when the calculation domain spans $0 < x < 1$. We have used the initial conditions from Zhang & MacFadyen (2006) with adiabatic index $\Gamma = 5/3$ as follows.

Left state ($0 < x < 0.5$): $\rho_L = 1$, $P_L = 10^3$, $v_{x,L} = 0$ and $v_{z,L} = 0.99c$.

Right state ($0.5 < x < 1$): $\rho_R = 1$, $P_R = 10^{-2}$, $v_{x,R} = 0$ and $v_{z,R} = 0.99c$.

Figure 18 denotes numerical and analytic solutions of this problem at $t = 0.6$. Analytic solutions in the appendix are calculated with the code of Giacomazzo & Rezzolla (2006). Upper and lower panels correspond to the case with $\Delta x = 10^{-3}$ and 2×10^{-5} , respectively. In the low-resolution run, we can find the diffusion of the contact discontinuity. The position of the right-going shock front is not correctly captured. On the contrary, the left-going rarefaction wave is resolved with good accuracy. In the high-resolution run, the numerical solution captures the analytic solution well, although there is some undershoot in the transverse velocity v_z at the contact discontinuity.

A.2. One-dimensional Hydrodynamic Relativistic Jet Model

We have also performed another convergence test using our jet model parameters in 1D (x -direction) cartesian coordinate using a uniform high resolution of $\Delta x = 2 \times 10^{-5}$ and the resolution of $\Delta x = 10^{-3}$ adopted in section 2. We set the initial conditions as follows.

Left state ($0 < x < 0.5$): $\rho_L = 0.1$, $P_L = 1$, $v_{x,L} = 0$ and $v_{z,L} = 0.99c$.

Right state ($0.5 < x < 1$): $\rho_R = 1$, $P_R = 0.1$, $v_{x,R} = 0$ and $v_{z,R} = 0$.

Figure 19 shows the numerical and analytic solutions of our jet model at $t = 0.1$ in the case with $\Delta x = 2 \times 10^{-5}$. The numerical solution resolves the hydrodynamic structure of the analytic solution very well. In the case with $\Delta x = 10^{-3}$, the position of the right-propagating shock front is not correctly captured while the numerical solution is able to capture the hydrodynamic structure of the rarefaction wave and the contact discontinuity as shown in Figure 20. In this paper, we focus on the interaction of rarefaction waves excited at the jet-ambient medium interface. Since the shock wave propagates outward from the jet-ambient medium interface, the interaction of rarefaction

waves inside the jet is not affected by the outward-going shock wave.

In our calculations in section 2, shock waves are excited inside the cylindrical jet. In order to investigate the effect of these shock waves, we have compared results of the calculation we performed in section 2 to those of the high-resolution calculation, in which a uniform grid with the grid size $\Delta r = 2 \times 10^{-5}$ is adopted in the cylindrical coordinate. Figure 21 illustrates the temporal evolution of (a) the jet width, (b) the maximum and (c) the average Lorentz factor in the jet in both numerical runs. Note that horizontal axis corresponds to the time for the duration $0 < t < 100$ demonstrated in Figure 7. The jet width in the case with $\Delta r = 10^{-3}$ is up to a factor 1.07 larger than in the high-resolution case because of numerical diffusion of the contact discontinuity. This leads to a 2 percent decrease in the average Lorentz factor inside the jet compared to the high-resolution case. We can find, however, only small differences of the maximum Lorentz factor in the jet between these numerical runs. Therefore, our choice of resolution does not impact significantly on our main results.

REFERENCES

- Acciari, V. A., Aliu, E., Arlen, T., et al. 2009, *Science*, 325, 444
- Agudo, I., Gómez, J.-L., Martí, J.-M., et al. 2001, *ApJ*, 549, L183
- Aloy, M.-A., Gómez, J.-L., Ibáñez, J.-M., Martí, J.-M., Müller, E. 2000a, *ApJ*, 528, L85
- Aloy, M. A., Müller, E., Ibáñez, J. M., Martí, J. M., & MacFadyen, A. 2000b, *ApJ*, 531, L119
- Aloy, M. A., Martí, J.-M., Gómez, J.-L., et al. 2003, *ApJ*, 585, L109
- Aloy, M. A., Janka, H.-T., & Müller, E. 2005, *A&A*, 436, 273
- Aloy, M. A., & Rezzolla, L. 2006, *ApJ*, 640, L115
- Aloy, M. A., & Mimica, P. 2008, *ApJ*, 681, 84
- Bicknell, G. V., & Begelman, M. C. 1996, *ApJ*, 467, 597
- Blandford, R. D., & Payne, D. G. 1982, *MNRAS*, 199, 883
- Blandford, R. D. 2000, *Astronomy, physics and chemistry of H₃⁺*, 358, 811
- Bromberg, O., & Levinson, A. 2007, *ApJ*, 671, 678
- Daly, R. A., & Marscher, A. P. 1988, *ApJ*, 334, 539

- Ferrari, A. 1998, *ARA&A*, 36, 539
- Giacomazzo, B., & Rezzolla, L. 2006, *Journal of Fluid Mechanics*, 562, 223
- Giroletti, M., Giovannini, G., Feretti, L., et al. 2004, *ApJ*, 600, 127
- Gomez, J. L., Marti, J. M. A., Marscher, A. P., Ibanez, J. M. A., & Marcaide, J. M. 1995, *ApJ*, 449, L19
- Gomez, J. L., Marti, J. M. A., Marscher, A. P., Ibanez, J. M. A., & Alberdi, A. 1997, *ApJ*, 482, L33
- Junor, W., Biretta, J. A., & Livio, M. 1999, *Nature*, 401, 891
- Kohler, S., Begelman, M. C., & Beckwith, K. 2011, arXiv:1112.4843
- Komissarov, S. S., & Falle, S. A. E. G. 1997, *MNRAS*, 288, 833
- Komissarov, S. S., & Falle, S. A. E. G. 1998, *MNRAS*, 297, 1087
- Komissarov, S. S., Vlahakis, N., & Königl, A. 2010, *MNRAS*, 407, 17
- Kovalev, Y. Y., Lister, M. L., Homan, D. C., & Kellermann, K. I. 2007, *ApJ*, 668, L27
- Lazzati, D., Morsony, B. J., & Begelman, M. C. 2009, *ApJ*, 700, L47
- Lyutikov, M., & Blandford, R. 2003, arXiv:astro-ph/0312347
- Marti, J. M. A., Mueller, E., Font, J. A., Ibanez, J. M. A., & Marquina, A. 1997, *ApJ*, 479, 151
- Meliani, Z., & Keppens, R. 2009, *ApJ*, 705, 1594
- Mészáros, P. 2006, *Reports on Progress in Physics*, 69, 2259
- Mignone, A., & Bodo, G. 2005, *MNRAS*, 364, 126
- Mignone, A., & McKinney, J. C. 2007, *MNRAS*, 378, 1118
- Mimica, P., Aloy, M. A., Müller, E., & Brinkmann, W. 2005, *A&A*, 441, 103
- Mimica, P., Aloy, M.-A., Agudo, I., et al. 2009, *ApJ*, 696, 1142
- Mirabel, I. F., & Rodríguez, L. F. 1999, *ARA&A*, 37, 409
- Mizuno, Y., Hardee, P., Hartmann, D. H., Nishikawa, K.-I., & Zhang, B. 2008, *ApJ*, 672, 72
- Mizuta, A., Yamasaki, T., Nagataki, S., & Mineshige, S. 2006, *ApJ*, 651, 960

- Mizuta, A., & Aloy, M. A. 2009, *ApJ*, 699, 1261
- Morsony, B. J., Lazzati, D., & Begelman, M. C. 2007, *ApJ*, 665, 569
- Morsony, B. J., Lazzati, D., & Begelman, M. C. 2010, *ApJ*, 723, 267
- Nagakura, H., Ito, H., Kiuchi, K., & Yamada, S. 2011, *ApJ*, 731, 80
- Nalewajko, K., & Sikora, M. 2009, *MNRAS*, 392, 1205
- Norman, M. L., Winkler, K.-H. A., Smarr, L., & Smith, M. D. 1982, *A&A*, 113, 285
- Piran, T. 2004, *Reviews of Modern Physics*, 76, 1143
- Perucho, M., & Martí, J. M. 2007, *MNRAS*, 382, 526
- Sanders, R. H. 1983, *ApJ*, 266, 73
- Scheck, L., Aloy, M. A., Martí, J. M., Gómez, J. L., Müller, E. 2002, *MNRAS*, 331, 615
- Shibata, K., & Uchida, Y. 1986, *PASJ*, 38, 631
- Stawarz, Ł., Aharonian, F., Kataoka, J., et al. 2006, *MNRAS*, 370, 981
- Takahashi, T., Kataoka, J., Madejski, G., et al. 2000, *ApJ*, 542, L105
- Tchekhovskoy, A., Narayan, R., & McKinney, J. C. 2010, *New A*, 15, 749
- Uchida, Y., & Shibata, K. 1985, *PASJ*, 37, 515
- Zenitani, S., Hesse, M., & Klimas, A. 2010, *ApJ*, 712, 951
- Zhang, W., Woosley, S. E., & MacFadyen, A. I. 2003, *ApJ*, 586, 356
- Zhang, W., Woosley, S. E., & Heger, A. 2004, *ApJ*, 608, 365
- Zhang, W., & MacFadyen, A. I. 2006, *ApJS*, 164, 255

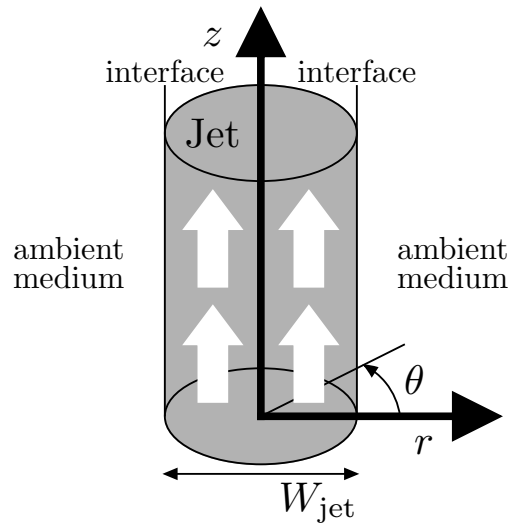


Fig. 1.— The numerical setting for our 1D simulations. A relativistically hot jet region is bounded by ambient gas. Derivatives of the physical variables in the z -direction and θ -direction are assumed to be zero. We calculate the evolution of the jet only in the radial direction.

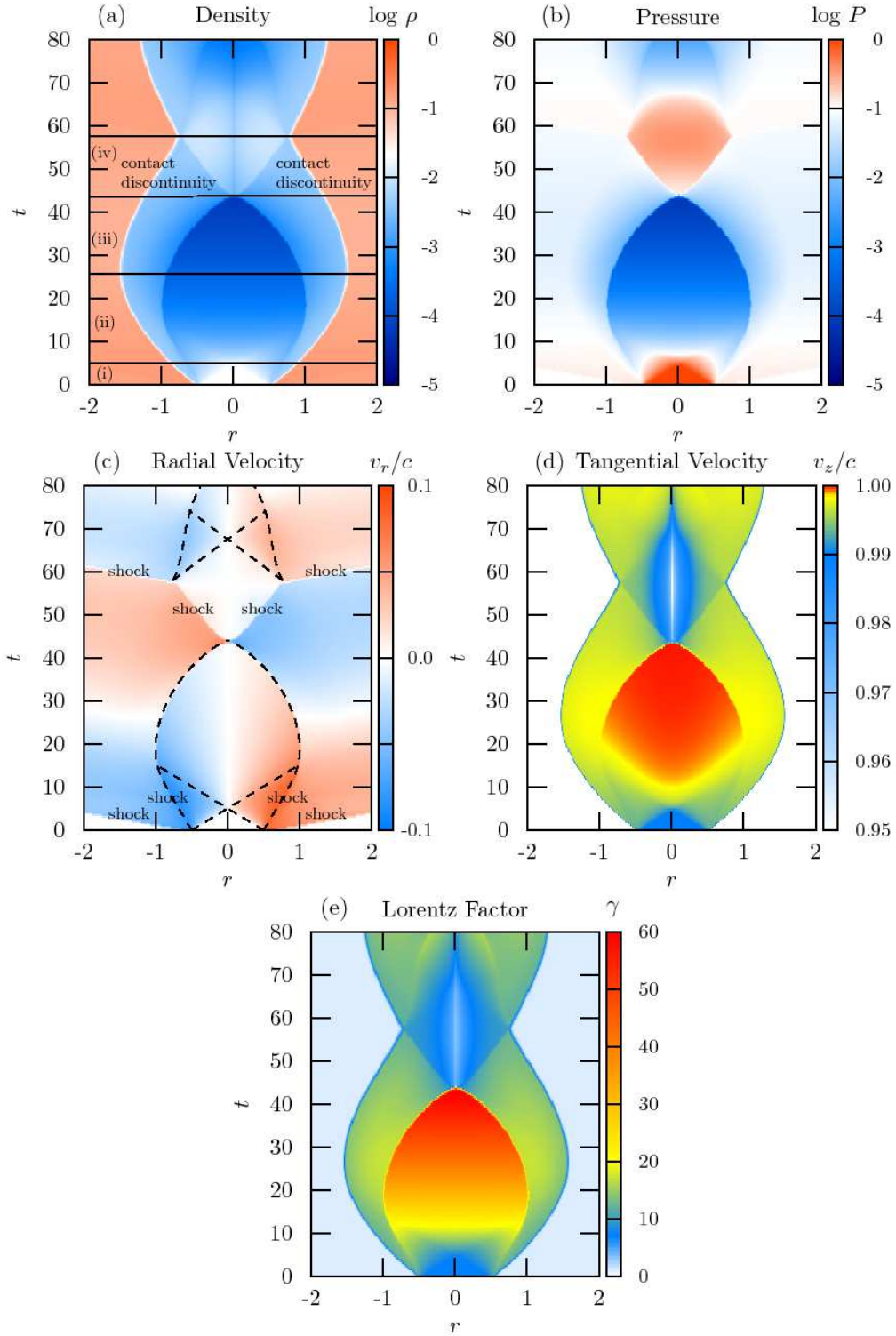


Fig. 2.— Temporal evolution of the jet-ambient medium system: (a) the density, (b) the pressure, (c) the radial velocity, (d) the tangential velocity and (e) the Lorentz factor. In panel (c), the rarefaction region is enclosed by dashed-lines. The tangential velocity of the ambient medium is zero in the panel (d). (A color version of this figure is available in the online journal.)

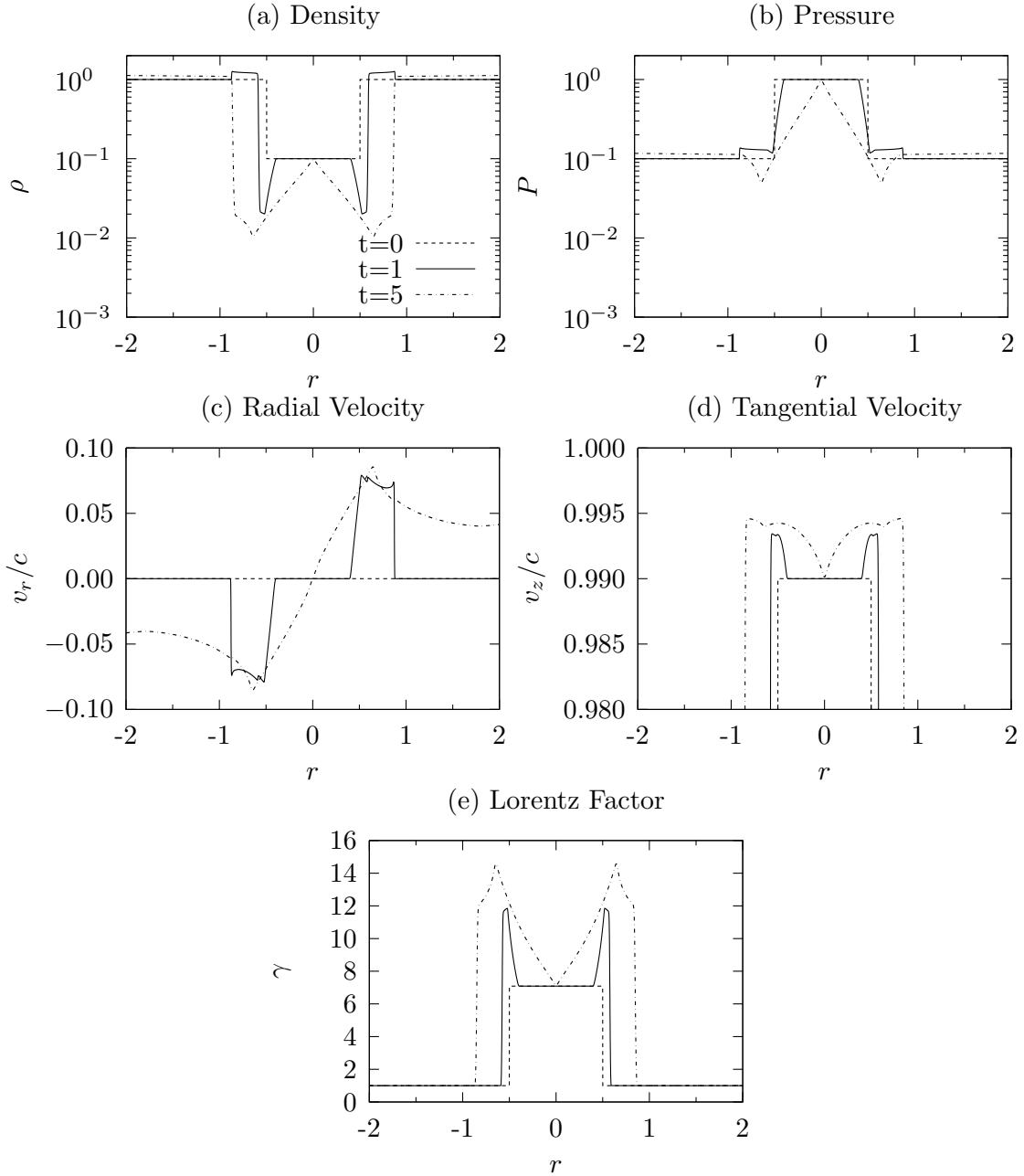


Fig. 3.— The spatial distribution of the jet-ambient medium system at $t = 0$ (dashed lines), $t = 1$ (solid lines) and $t = 5$ (dash-dotted lines): (a) the density, (b) the pressure, (c) the radial velocity, (d) the tangential velocity and (d) the Lorentz factor.

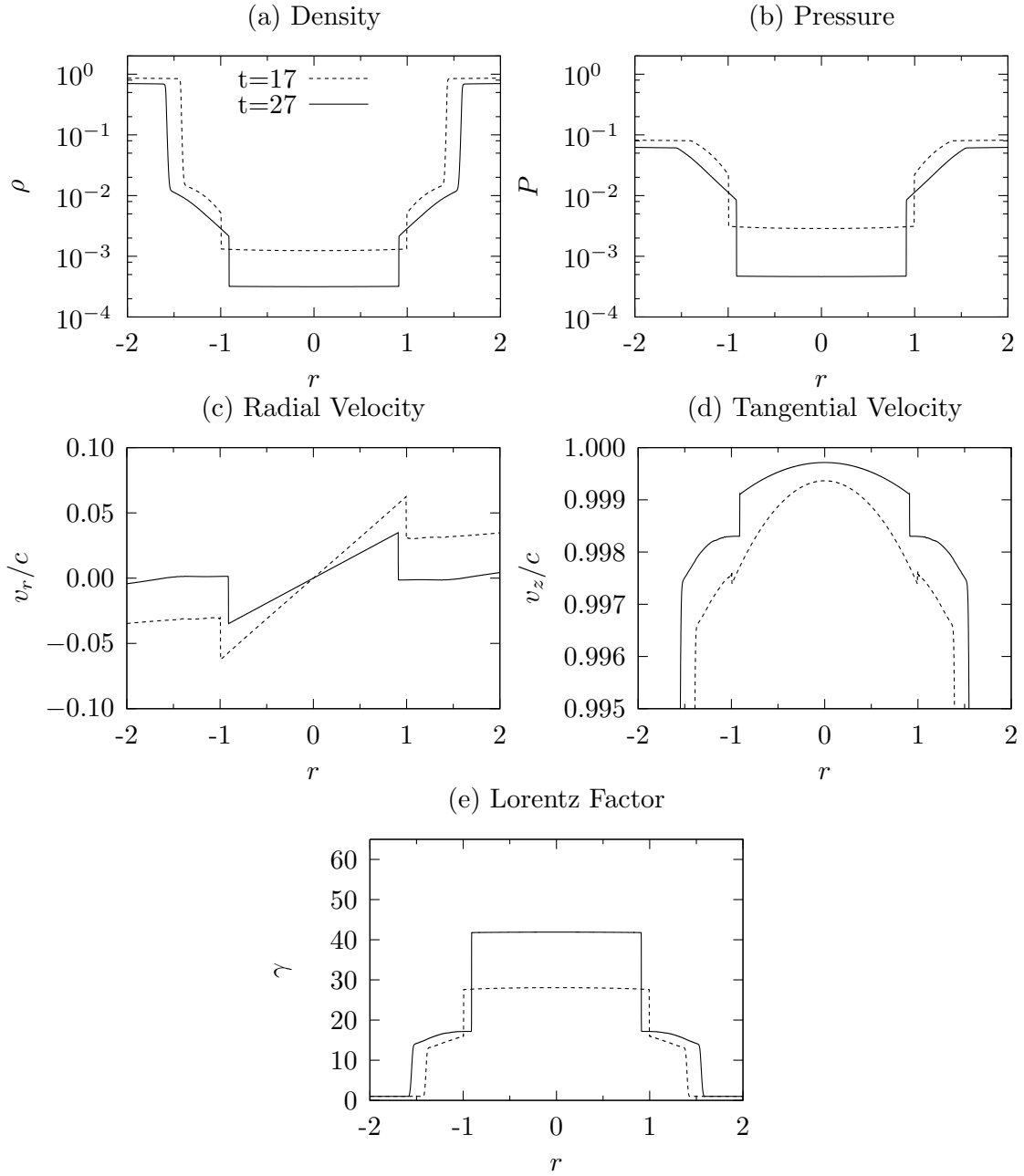


Fig. 4.— Same as Figure 3, but at $t = 17$ (dashed lines) and 27 (solid lines).

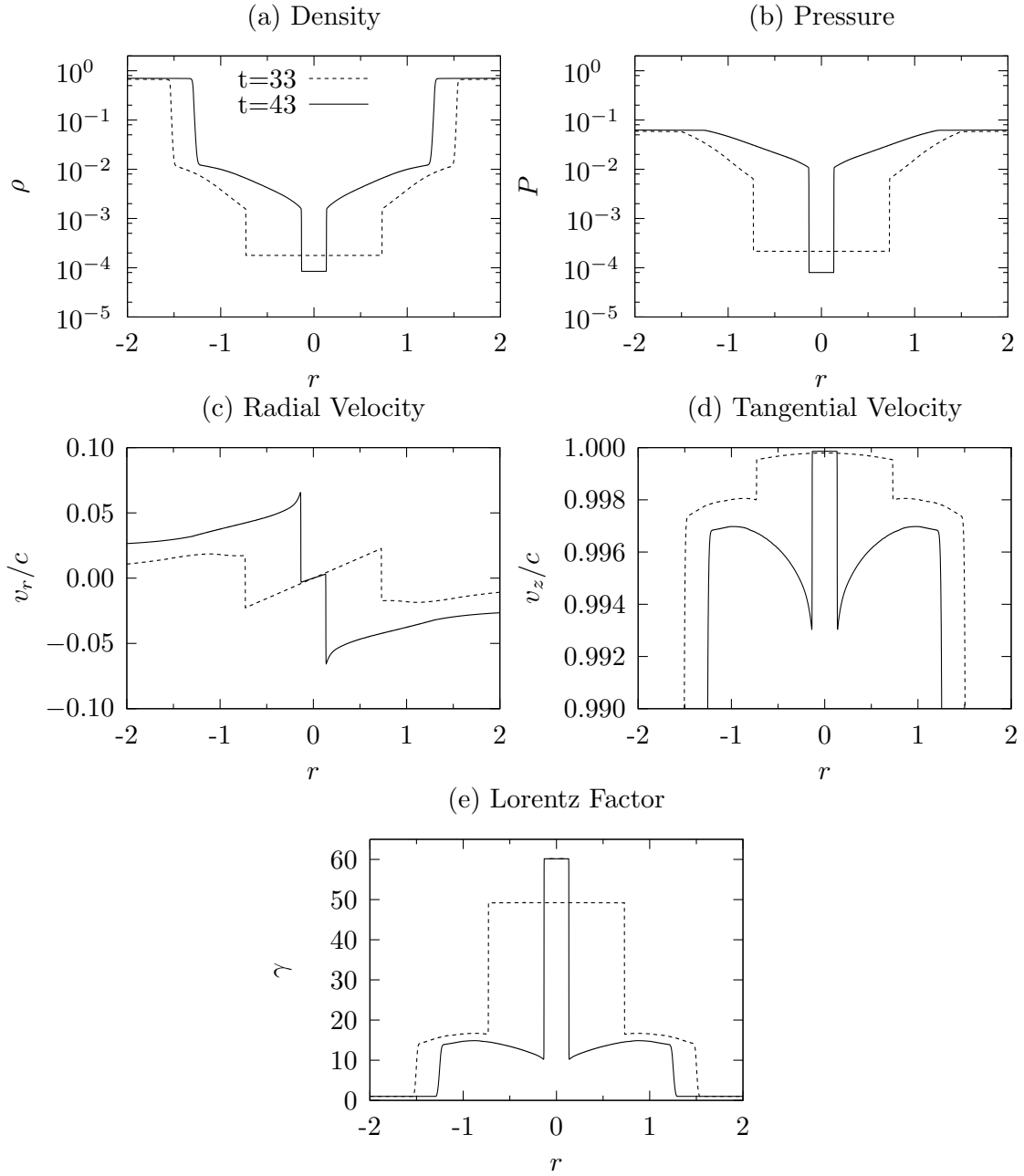


Fig. 5.— Same as Figure 3, but at $t = 33$ (dashed lines) and 43 (solid lines).

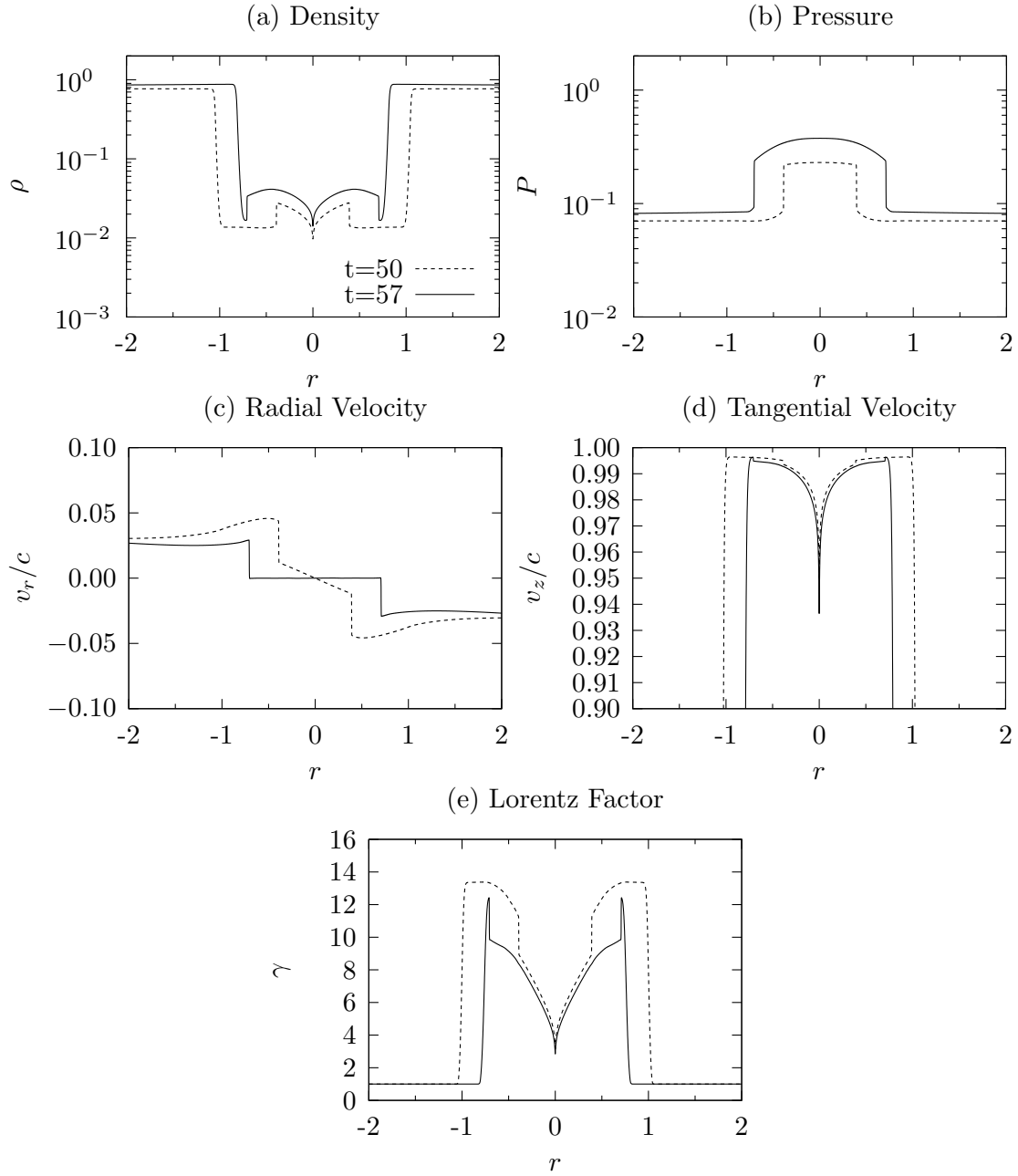


Fig. 6.— Same as Figure 3, but at $t = 50$ (dashed lines) and 57 (solid lines).

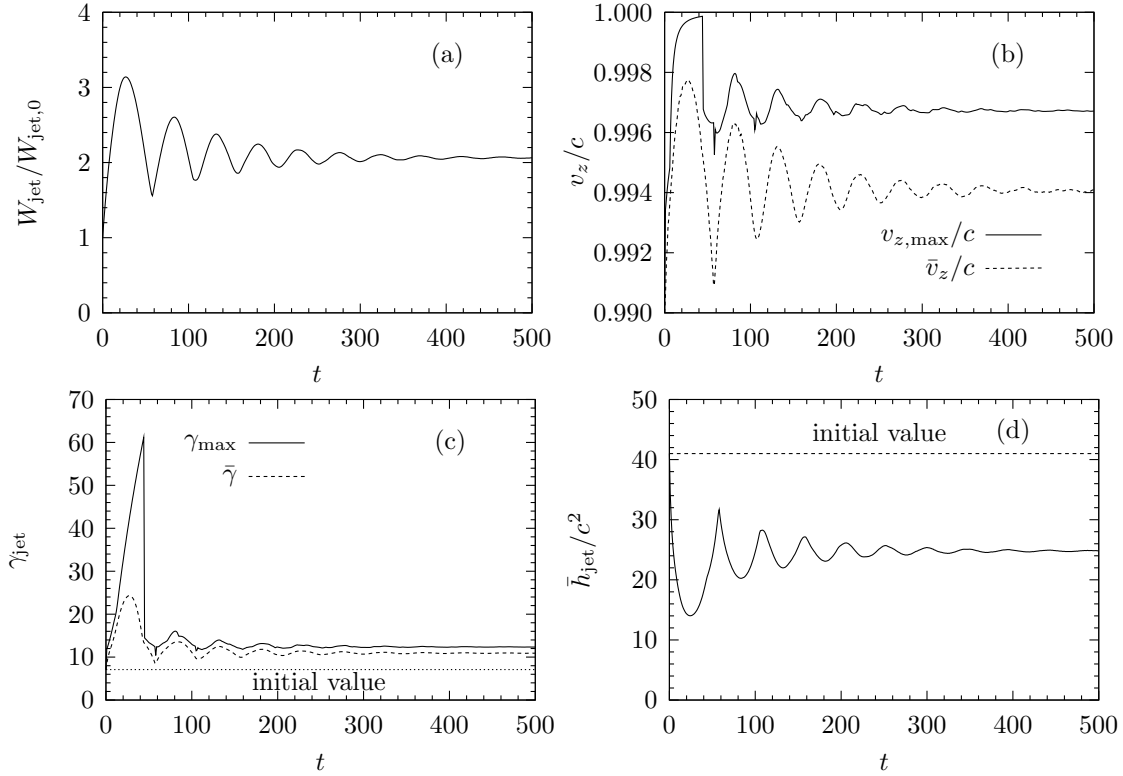


Fig. 7.— The temporal evolution of (a) the jet width, (b) the maximum and average of the tangential velocity ($v_{z,\max}$ and \bar{v}_z), (c) the maximum and average of the Lorentz factor (γ_{\max} and $\bar{\gamma}$), and (d) the average of the specific enthalpy in the jet. The initial Lorentz factor inside the jet is roughly 7 and shown by the dotted line in panel (c). However, the initial specific Lorentz factor of the jet is 41 and presented by a dashed line in panel (d).

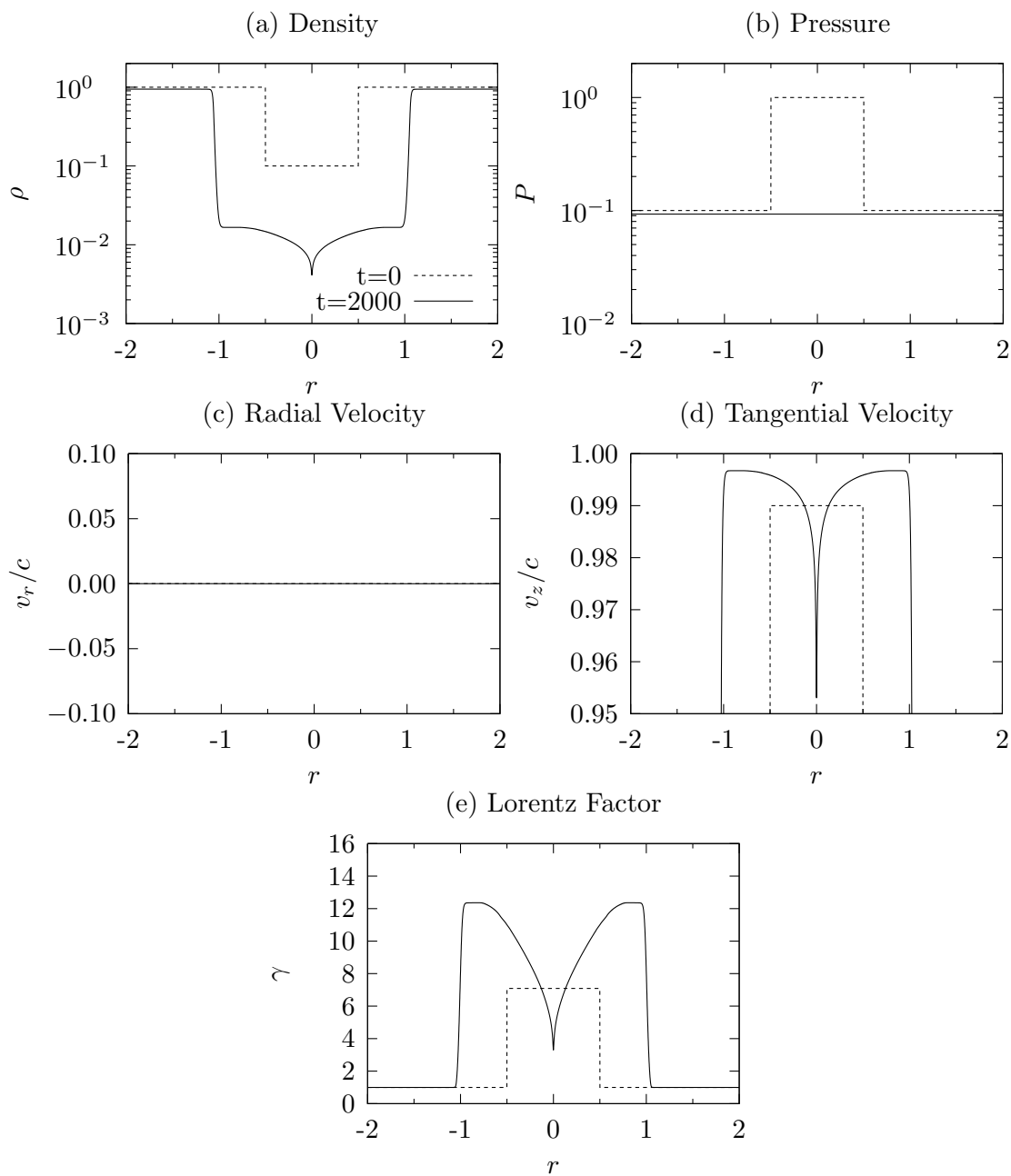


Fig. 8.— The spatial distribution of the initial non-equilibrium and final quasi-steady states of the jet: (a) the density, (b) the pressure, (c) the radial velocity, (d) the tangential velocity and (e) the Lorentz factor. The dashed and solid lines represent the initial ($t = 0$) and final ($t = 2000$) state, respectively.

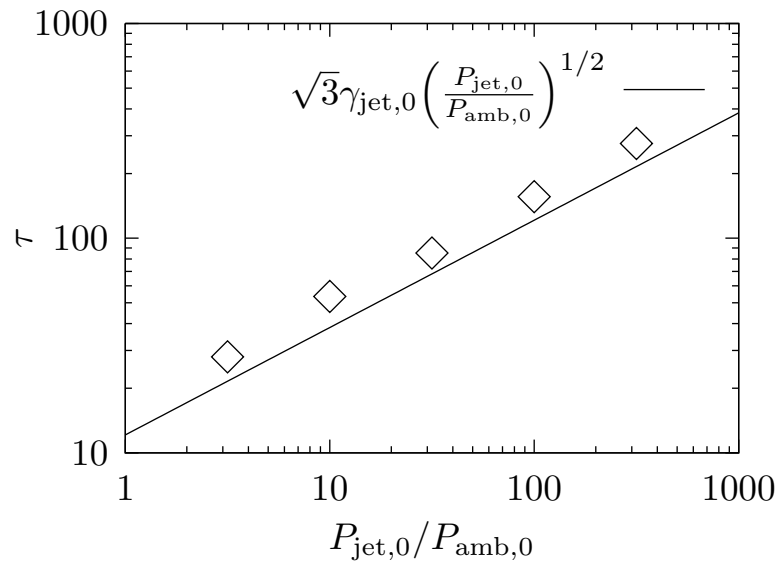


Fig. 9.— Relation between the oscillation time scale of the system and initial pressure ratio of the jet to the ambient gas (Equation (9)). Diamonds denote the oscillation time averaged over ten cycles for each parameter.

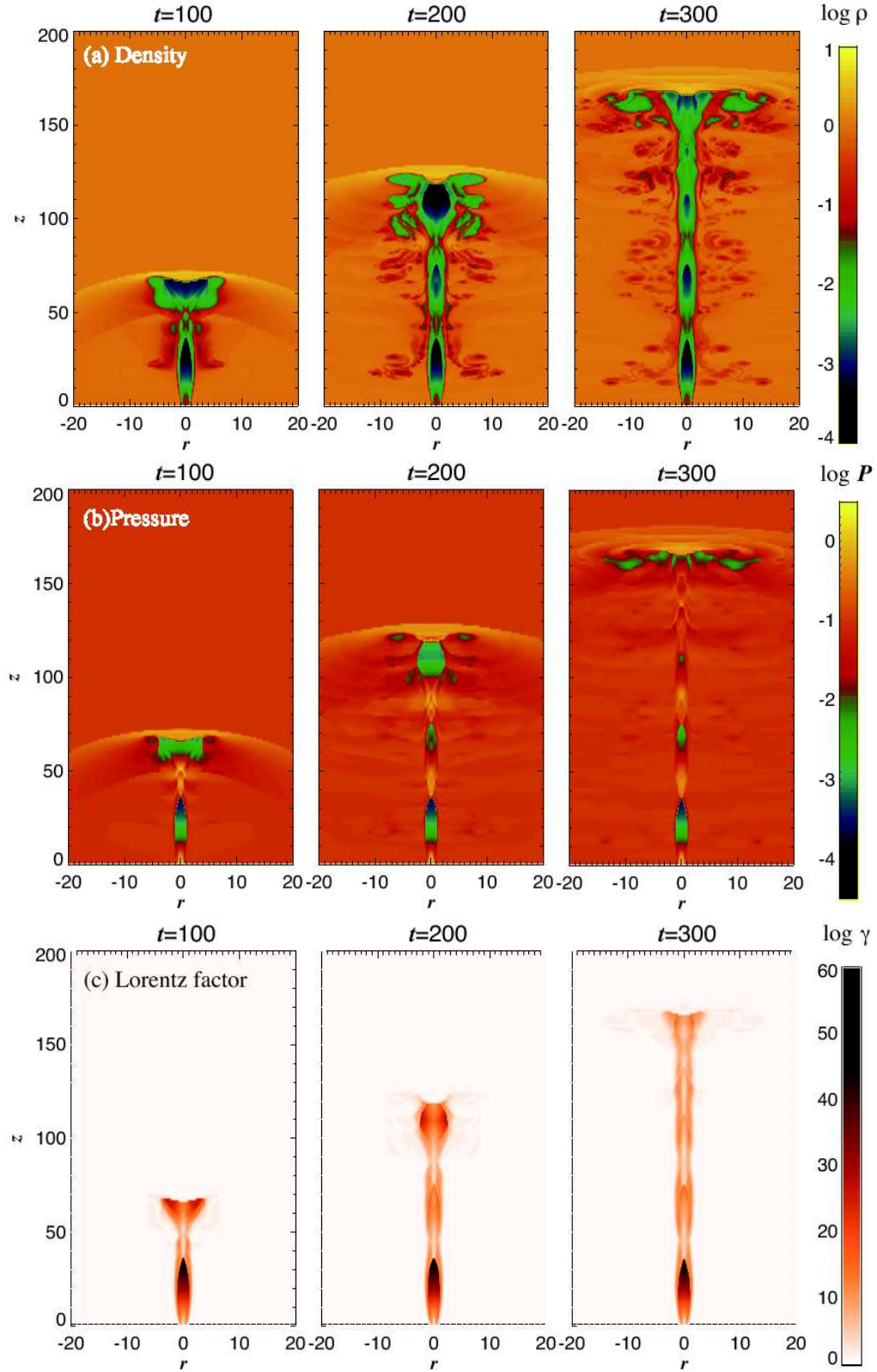


Fig. 10.— Time evolution of the injected relativistic jet into the uniform ambient medium: (a) the density, (b) the pressure and (c) the Lorentz factor. The left, middle, and right columns correspond to $t = 100$, 200, and 300, respectively. (A color version of this figure is available in the online journal.)

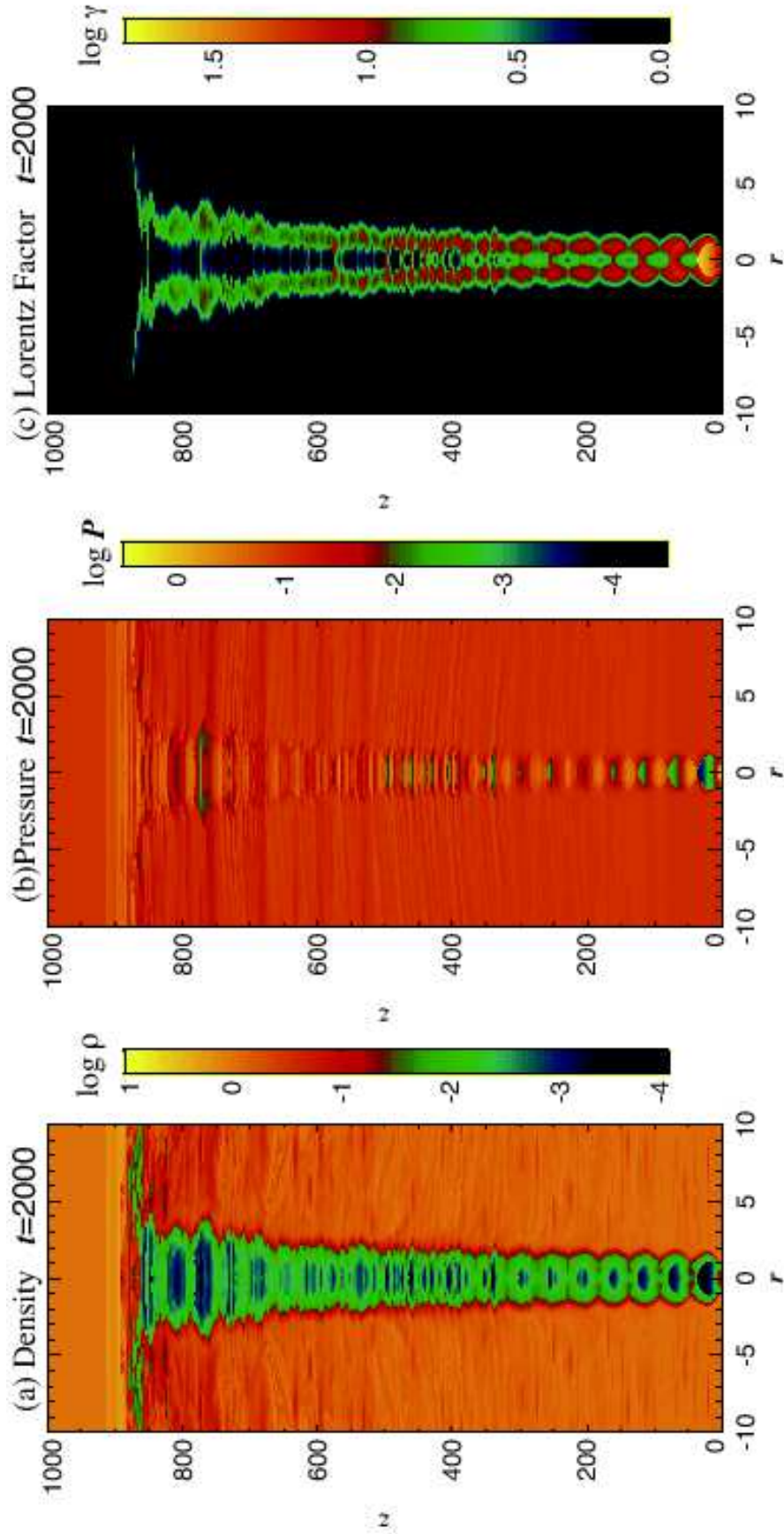


Fig. 11.— Snapshots of the spatial distribution of (a) the density, (b) the pressure and (c) the

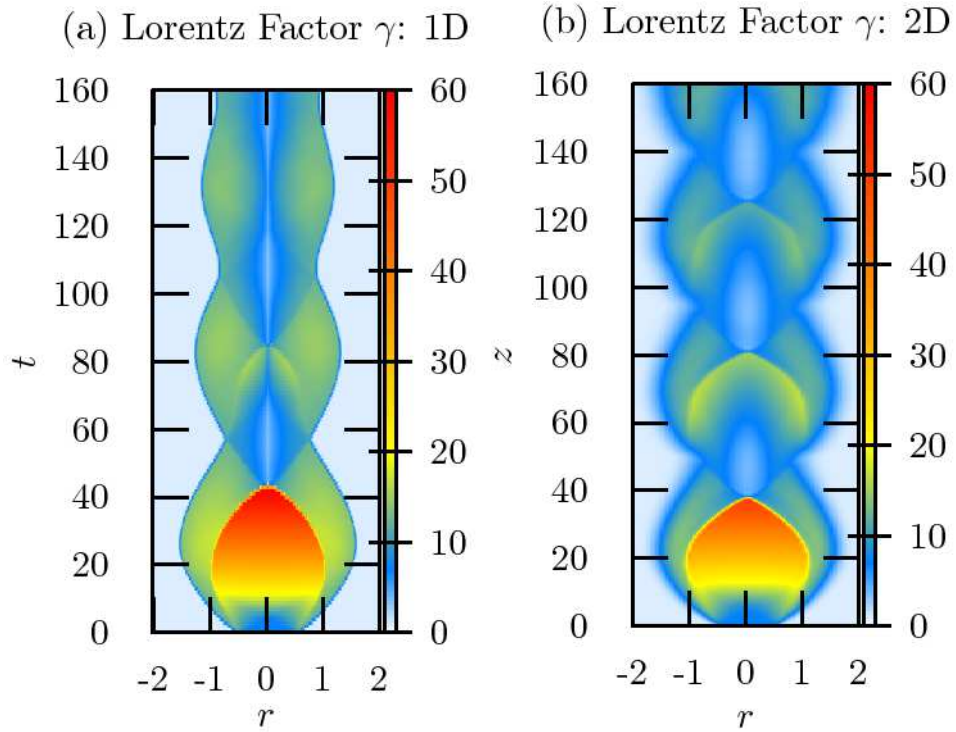


Fig. 12.— Left panel represents the time evolution of the Lorentz factor in the jet-ambient medium system of 1D simulation. Right panel demonstrates the spatial distribution of the Lorentz factor at $t = 2000$ in the uniform ambient model ($\alpha = 0$) of 2D simulation. (A color version of this figure is available in the online journal.)

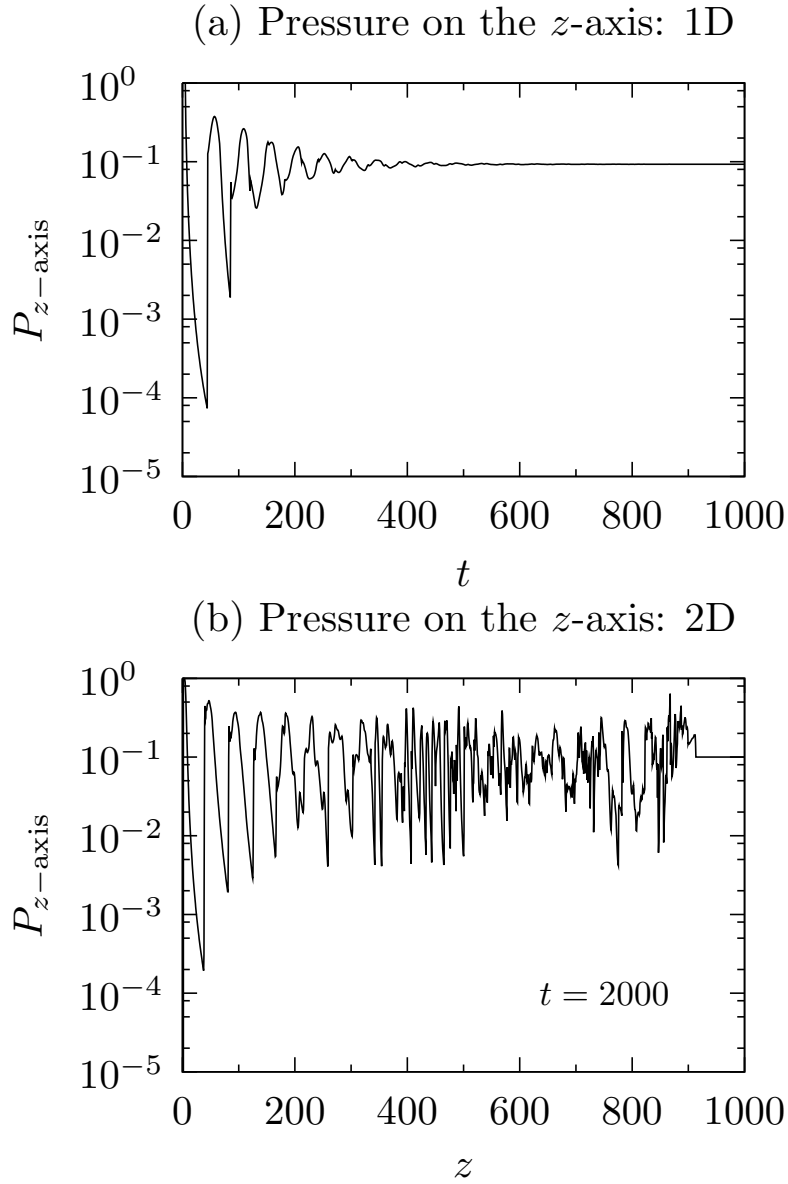


Fig. 13.— Panel (a): temporal evolution of the pressure at the z -axis in 1D simulation. Panel (b): spatial distribution of the pressure along the z -axis at $t = 2000$ in the uniform ambient model ($\alpha = 0$) of 2D simulation.

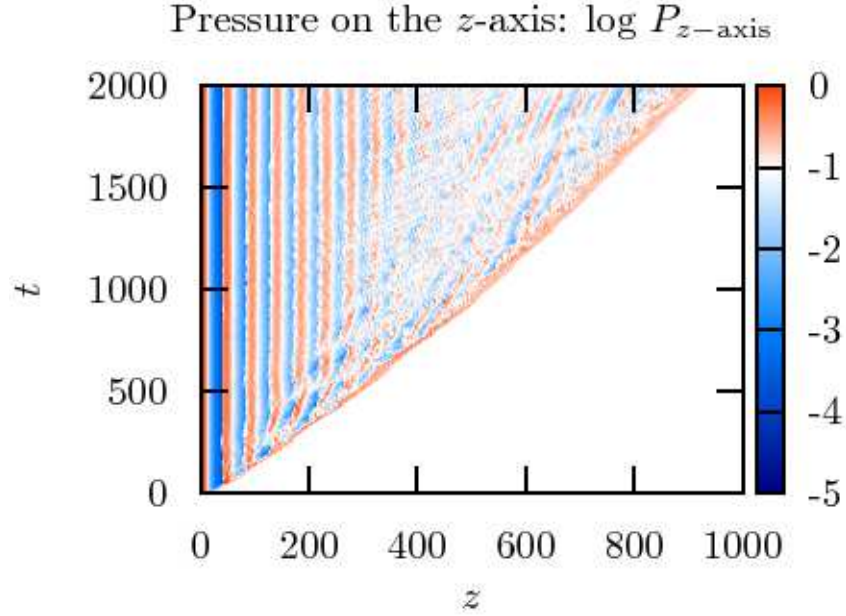


Fig. 14.— The time-distance diagram for the pressure on the z -axis in the uniform ambient model ($\alpha = 0$) of 2D simulation. (A color version of this figure is available in the online journal.)

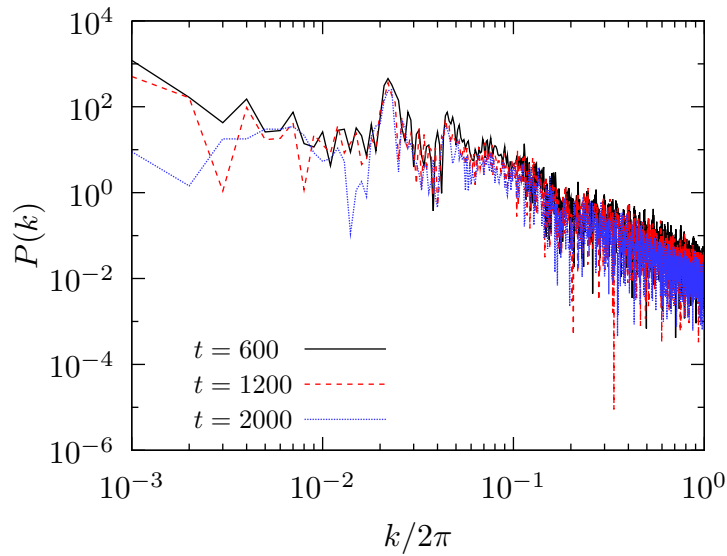


Fig. 15.— Temporal evolution of Fourier spectrum of the pressure measured along the jet axis $P(k) = \frac{1}{L_{\text{jet}}} \int_0^{L_{\text{jet}}} P_{z\text{-axis}}(z) \exp^{-ikz} dz$, where L_{jet} is the length of the jet in the propagation direction. The solid, dashed and dotted curves correspond to the case $t = 600$, 1200 and 2000 , respectively. (A color version of this figure is available in the online journal.)

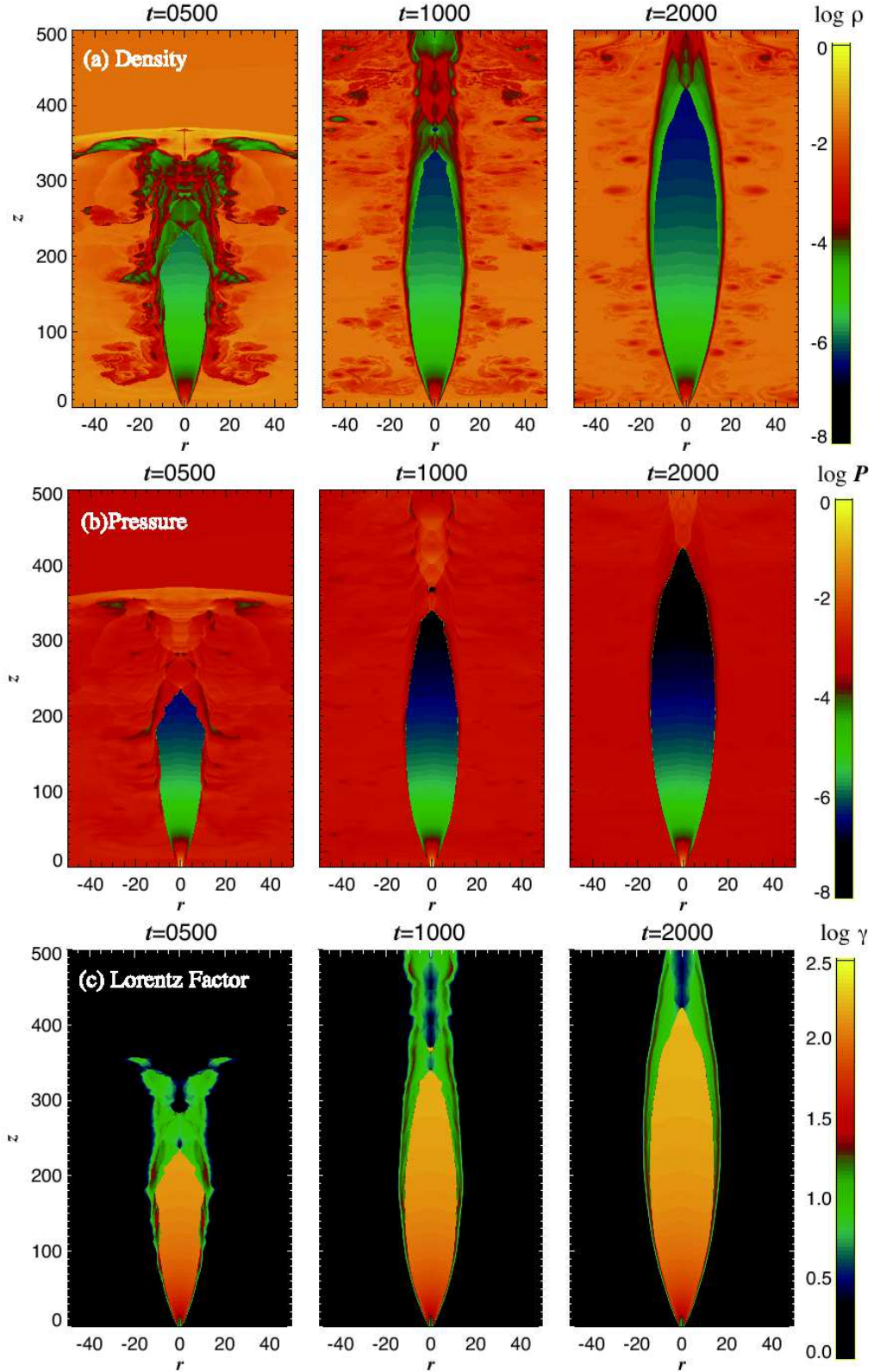


Fig. 16.— Time evolution of the injected relativistic jet in the power-law pressure distribution model where the power-law index $\alpha = 0.8$: (a) the density, (b) the pressure and (c) the Lorentz factor. The left, middle, and right columns correspond to $t = 500$, 1000 , and 2000 , respectively. (A color version of this figure is available in the online journal.)

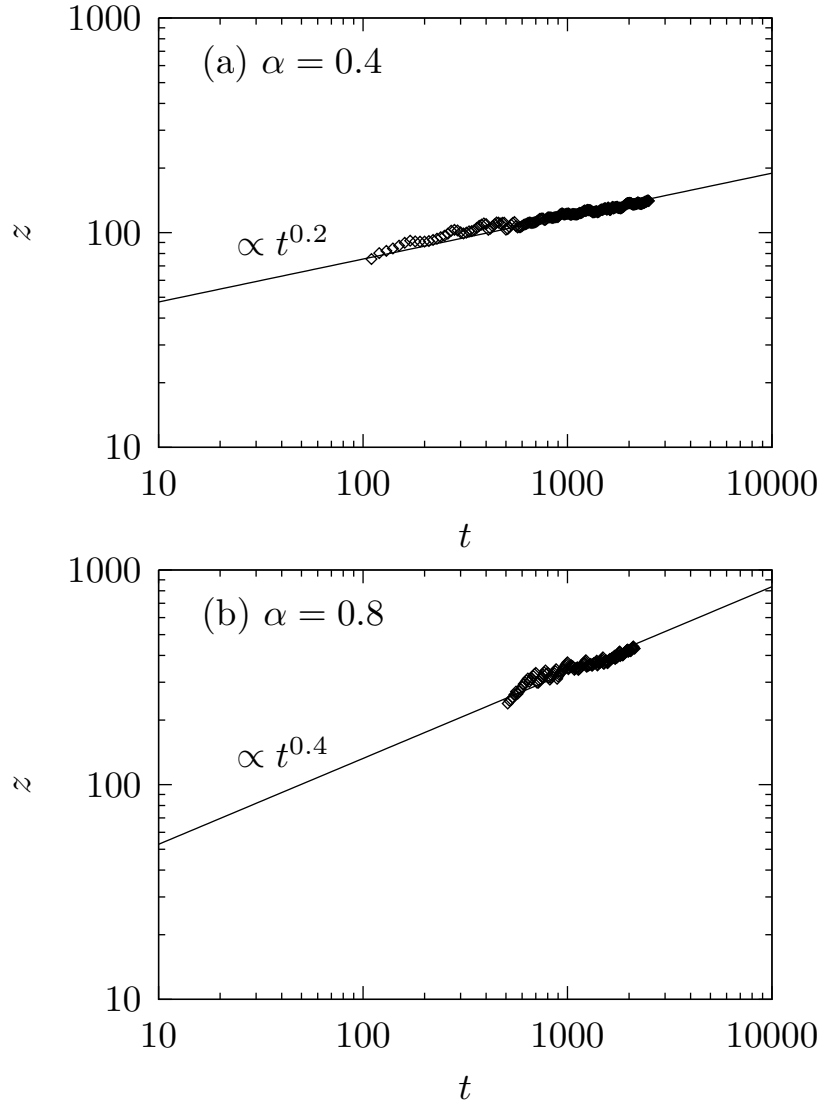


Fig. 17.— Time trajectory of the position of the cusp of the first reconfinement region on the z-axis is depicted by diamonds. Solid lines demonstrate the scaling law $\lambda \propto t^{\alpha/2}$ we derived in section 3.2 where λ and α are the length of the cusp-shaped reconfinement region along the z-axis and the index of the power-law pressure distribution of the ambient medium, respectively. Panel (a) and (b) correspond to the case with $\alpha = 0.4$ and $\alpha = 0.8$.

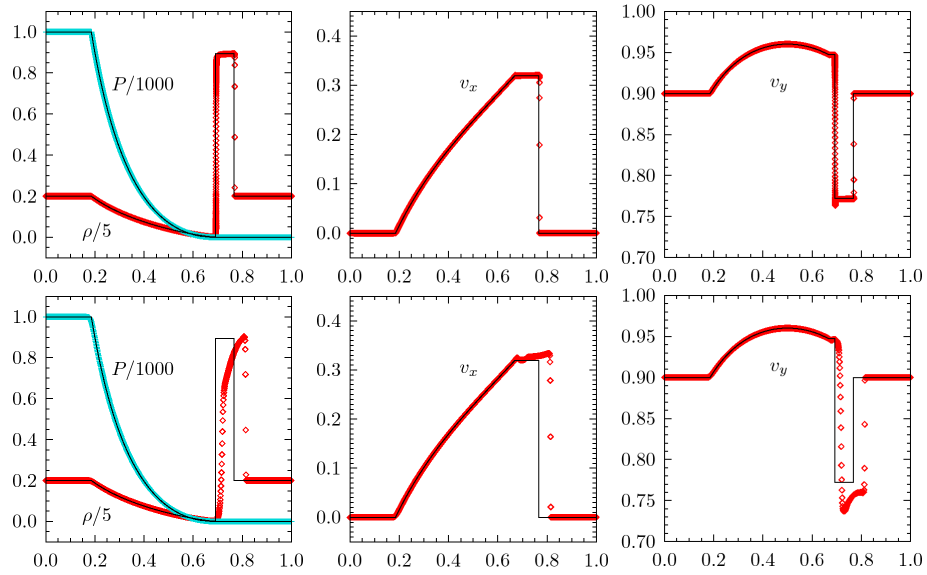


Fig. 18.— Solutions of 1D Riemann problem with large transverse velocity at $t = 0.6$. Upper and lower panels correspond to the high-resolution ($\Delta x = 2 \times 10^{-5}$) and low-resolution ($\Delta x = 10^{-3}$) cases, respectively. Diamonds and crosses represent the numerical solution while solid lines are analytic solution. (A color version of this figure is available in the online journal.)

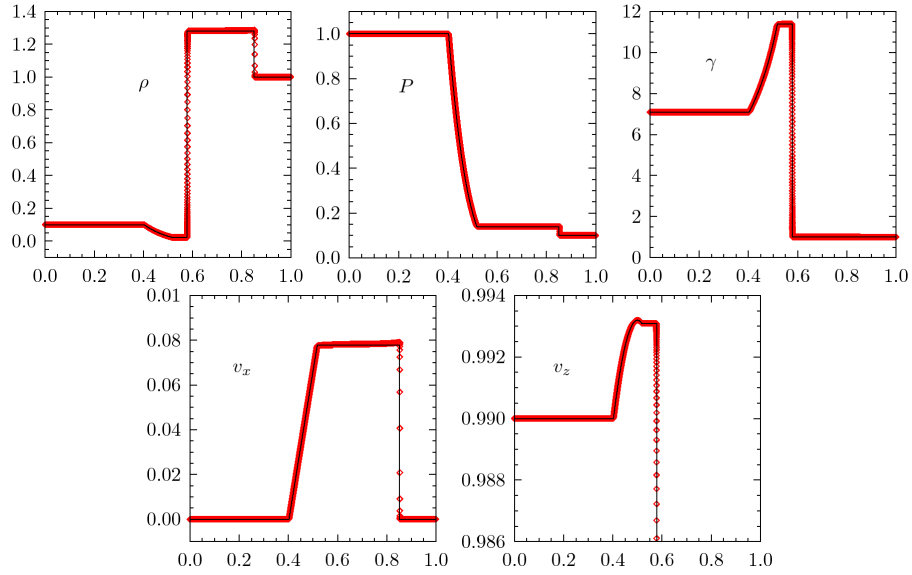


Fig. 19.— Solutions of Riemann problem of our jet model in 1D (x-direction) cartesian coordinate with the resolution of $\Delta x = 2 \times 10^{-5}$. Diamonds and solid lines illustrate the numerical and analytic solutions, respectively. (A color version of this figure is available in the online journal.)

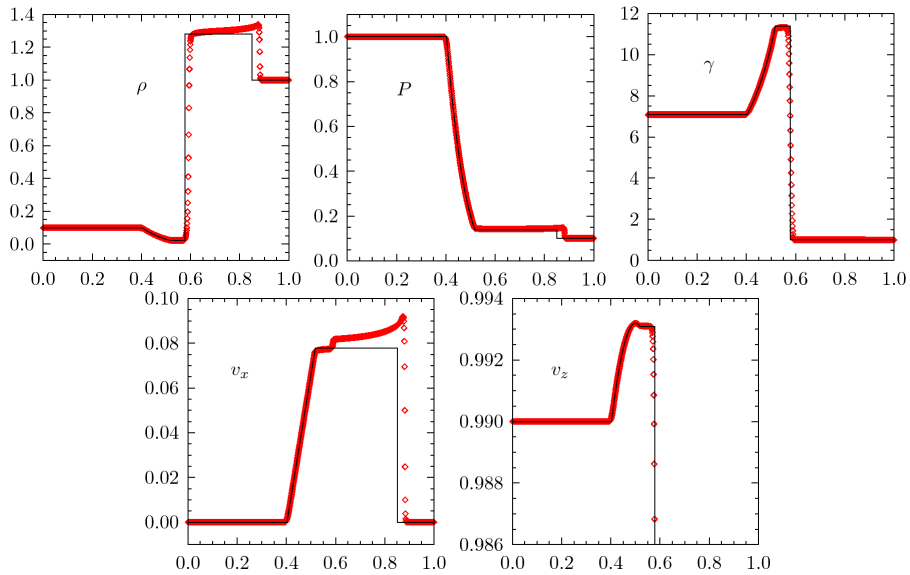


Fig. 20.— Same as Figure 19 but the case with $\Delta x = 10^{-3}$. (A color version of this figure is available in the online journal.)

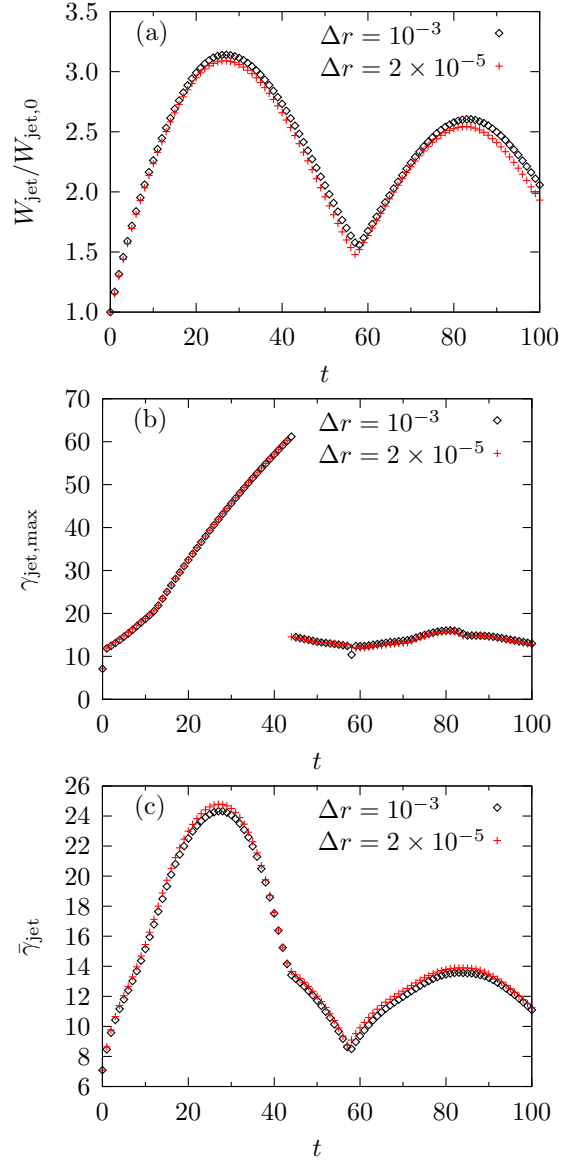


Fig. 21.— Temporal evolution of (a) the jet width, (b) the maximum and (c) the average Lorentz factor in the jet. Diamonds and crosses correspond to the resolution of $\Delta x = 10^{-3}$ and $\Delta x = 2 \times 10^{-5}$, respectively. (A color version of this figure is available in the online journal.)